Effects of ozone isotopologue formation on the clumped-isotope composition of atmospheric O_2

Laurence Y. Yeung,[1,*] Lee T. Murray,[2] Asmita Banerjee,[1] Xin Tie,[2] Yuzhen Yan,[1] Elliot L. Atlas,[3] Sue M. Schauffler,[4] and Kristie A. Boering[5]

[1]Department of Earth, Environmental and Planetary Sciences, Rice University, Houston, TX 77005

[2]Department of Earth and Environmental Sciences, University of Rochester, Rochester, NY

[3]Division of Marine and Atmospheric Chemistry, University of Miami, Miami, FL

[4]National Center for Atmospheric Research, Boulder, CO

[5]Departments of Chemistry and Earth and Planetary Science, University of California, Berkeley, CA

[*]correspondence: lyeung@rice.edu

Abstract

Tropospheric $^{18}O^{18}O$ is an emerging proxy for past tropospheric ozone and free-tropospheric temperatures. The basis of these applications is the idea that isotope-exchange reactions in the atmosphere drive $^{18}O^{18}O$ abundances toward isotopic equilibrium. However, previous work used an offline box-model framework to explain the $^{18}O^{18}O$ budget, approximating the interplay of atmospheric chemistry and transport. This approach, while convenient, has poorly characterized uncertainties. To investigate these uncertainties, and to broaden the applicability of the $^{18}O^{18}O$ proxy, we developed a scheme to simulate atmospheric $^{18}O^{18}O$ abundances (quantified as Δ_{36} values) online within the GEOS-Chem chemical transport model. These results are compared to both new and previously published atmospheric observations from the surface to 33 km. Simulations using a simplified O_2 isotopic equilibration scheme within GEOS-Chem show quantitative agreement with measurements only in the middle stratosphere; modeled Δ_{36} values are too high elsewhere. Investigations using a comprehensive model of the O-O_2-O_3 isotopic photochemical system and proof-of-principle experiments suggest that the simple equilibration scheme omits an important pressure dependence to Δ_{36} values: the anomalously efficient titration of $^{18}O^{18}O$ to form ozone. Incorporating these effects into the online Δ_{36} calculation scheme in GEOS-Chem yields quantitative agreement for all available observations. While this previously unidentified bias affects the atmospheric budget of $^{18}O^{18}O$ in O_2, the modeled change in the mean tropospheric Δ_{36} value since 1850 C.E. is only slightly altered; it is still quantitatively consistent with the ice-core Δ_{36} record, implying that the tropospheric ozone burden increased less than ~40% over the twentieth century.

9937 Words (main text)

591 Words (figure captions)

10 Figures

1 Table

Plain Language Summary

Oxygen in the air is constantly being broken apart and remade. Its constituent atoms are shuffled around by light-induced chemical reactions, which cause changes in the number of heavy oxygen atoms that are bound together. The number of these heavy-atom "clumps" is sensitive to air temperatures and the presence of air pollution; hence, their variations are being used to understand past high-altitude temperatures and atmospheric chemistry. This study incorporates oxygen clumping into an atmospheric chemistry model and compares the results to measurements of oxygen clumping in the atmosphere. We find that the model can explain all the modern-day measurements (from the surface to 33 km altitude), but only if the broader fates of oxygen atoms—i.e., their incorporation into other molecules beyond O_2—are considered. Simulations of the preindustrial atmosphere are also generally consistent with snapshots of the ancient atmosphere obtained from O_2 trapped in ice cores. The developments described herein will thus enable models to simulate heavy oxygen-atom clumping in past cold and warm climates and enable simulated high-altitude atmospheric changes to be evaluated directly against ice-core snapshots of the ancient atmosphere.

1. Introduction

Odd oxygen [$O(^3P)$, $O(^1D)$, and O_3] is a key component of the atmosphere's oxidizing capacity. As such, tracing its evolution over time may provide better constraints on greenhouse-gas lifetimes, stratosphere-troposphere coupling, biosphere-atmosphere interactions, and radiative forcing in the past. Moreover, elevated odd-oxygen concentrations in the upper troposphere and stratosphere mean that a globally integrated record of odd-oxygen chemistry would be a unique window on the high-altitude atmosphere of the past, not just in terms of chemistry but also climate [*Thompson et al.*, 1998; *Tripati et al.*, 2014; *Yeung et al.*, 2016; *Loomis et al.*, 2017]. Observational constraints on temperatures of the ancient high-altitude atmosphere, for example, would bring new insights on Earth's past energy balance.

The short lifetime of odd-oxygen species, however, precludes their direct preservation in traditional atmospheric archives. Interrogating the past variability of atmospheric odd oxygen thus requires the use of proxies and models [*Alexander et al.*, 2003; *Murray et al.*, 2014; *Alexander and Mickley*, 2015; *Geng et al.*, 2017; *Yeung et al.*, 2019]. For example, hydrogen peroxide is a stable product of odd-oxygen chemistry (via HO_2 self-reaction) that is preserved in ice cores, but its sensitivity to post-depositional alteration limits the scenarios under which its variations reflect atmospheric odd-oxygen changes [*Frey et al.*, 2006]. Another proxy is the $^{15}N/^{14}N$ ratio of snow-bound nitrate, which is sensitive to the local ultraviolet flux. It can offer insight on the local atmospheric column density of O_3 if the local accumulation rate and optical depth in the snow are known [*Frey et al.*, 2009; *Ming et al.*, 2020; *Winton et al.*, 2020]; however, anthropogenic changes to nitrogen cycling can overprint the these signals [*Hastings et al.*, 2009; *Geng et al.*, 2014]. A third proxy is based on the transfer of unique O_3-derived ^{17}O enrichments, primarily to nitrate and sulfate species. It can provide constraints on the relative importance of O_3, OH, and HO_2 oxidation pathways, but interpretations are often model-dependent [*Alexander et al.*, 2009; *Kunasek et al.*, 2010; *Sofen et al.*, 2011; *Sofen et al.*, 2014; *Geng et al.*, 2017]. Furthermore, all these approaches are only sensitive to local odd-oxygen variability; global trends are not accessible.

Recently, *Yeung et al.* [2019] applied a new proxy for odd-oxygen chemistry preserved in the ice-core record that offers a broader view. It is based on the proportional abundance of $^{18}O^{18}O$ in tropospheric O_2 (quantified as Δ_{36} values; see Section 2), which is linked to odd-oxygen chemistry through $O(^3P) + O_2$ isotope-exchange reactions. The subtle decrease in tropospheric Δ_{36} value occurring over the twentieth century was interpreted to reflect a change in odd-oxygen chemistry, namely, an increase in the tropospheric O_3 burden. The inferred magnitude of the increase (<40%) is in broad agreement with predictions made by state-of-the-art atmospheric chemistry models [*Yeung et al.*, 2019].

Temporal variations in tropospheric Δ_{36} values can be understood within a two-box framework, with separate tropospheric and stratospheric boxes [*Yeung et al.*, 2016]. Isotope-exchange reactions occur within each box, and mass is exchanged between them. Tropospheric chemistry leads to lower Δ_{36} values

than stratospheric chemistry because of the difference in characteristic temperatures: $O(^3P) + O_2$ isotope exchange at warmer temperatures generally yields smaller $^{18}O^{18}O$ enrichments, and thus lower Δ_{36} values, than isotope exchange at cold temperatures [*Yeung et al.*, 2012]. The tropospheric signal is well mixed on annual timescales, incorporating changes in stratospheric inputs on sub-decadal timescales [*Yeung et al.*, 2016]. Tropospheric Δ_{36} values therefore reflect the cumulative effects of isotope-exchange chemistry occurring in the troposphere (~3/4 of the signal) modulated by the input of high-Δ_{36} stratospheric air (~1/4 of the signal). An increase in the rate of $O(^3P) + O_2$ reactions in the troposphere, e.g., caused by increase in mean $O(^3P)$ concentration, leads to a decrease in tropospheric Δ_{36} values at steady state. Because the mean tropospheric $O(^3P)$ concentration is proportional to the O_3 burden (and has a negligible dependence on other atomic oxygen sources), tropospheric Δ_{36} values have been used as a proxy for past changes in the tropospheric O_3. A warming of the troposphere would also lower the mean tropospheric Δ_{36} value by lowering the characteristic tropospheric Δ_{36} values toward which isotope-exchange reactions drive O_2.

Yet, important details of the global Δ_{36} budget remain uncertain. Previous quantitative estimates of atmospheric Δ_{36} variations were facilitated by global 3-D chemical transport model simulations of $O(^3P)$ concentrations, but the Δ_{36} calculations were still performed offline, i.e., without direct coupling of atmospheric chemistry, mixing, and transport [*Yeung et al.*, 2016; *Yeung et al.*, 2019]. The expense of isotopologue-specific chemistry—e.g., the O-O_2-O_3 photochemical system itself requires >300 additional, highly stiff reactions to represent—renders explicit online calculation of $^{18}O^{18}O$ variations impractical.

A simplified treatment of the relevant O_2 isotopologue photochemistry is possible, however, because laboratory studies indicate that the approach of Δ_{36} values toward photochemical steady state can be described by pseudo-first-order kinetics [*Yeung et al.*, 2014]. Isotope-exchange reactions between $O(^3P)$ and O_2 at low pressures (e.g., 1 – 2 mbar) drive isotopologue abundances toward isotopic equilibrium, but the uncertainty in their kinetics is large, particularly at the low temperatures relevant for the upper troposphere and stratosphere (Fig. 1, left). Moreover, isotope effects in O_3 formation could be important—particularly the anomalous enrichments in $^{18}O^{18}O$-containing O_3 isotopologues, which also vary with temperature and pressure (Fig. 1, right) [*Mauersberger*, 1981; *Heidenreich and Thiemens*, 1983; *Thiemens and Heidenreich*, 1983; *Guenther et al.*, 1999; *Mauersberger et al.*, 1999; *Gao and Marcus*, 2001; *Janssen et al.*, 2003]. While imperfect, parameterization of these effects may offer a practical balance between accuracy and computational cost that allows Δ_{36} variations to be simulated online.

In this manuscript, we use new high-precision Δ_{36} measurements from the modern atmosphere spanning a range of latitudes in the Northern Hemisphere to evaluate two different online Δ_{36} calculation schemes within the GEOS-Chem chemical transport model. The first scheme considers only O_2 isotopic equilibration at *in situ* temperatures, using rates determined by local $O(^3P)$ concentrations and $O(^3P) + O_2$

isotope-exchange rate coefficients, while the second scheme includes a temperature- and pressure-dependent parameterization for the effects of O_3 formation. Furthermore, we compare the results of online and offline Δ_{36} calculation schemes to improve our understanding of the Δ_{36} budget and interpretations of Δ_{36} changes in the recent atmospheric record.

2. Methods

2.1 Measurements of new upper-tropospheric and lower-stratospheric samples

Twenty-three whole-air samples were collected from the NASA ER-2 aircraft during the Studies of Emissions, Atmospheric Composition, Clouds and Climate Coupling by Regional Surveys (SEAC^{4}RS) campaign [*Lueb et al.*, 1975; *Toon et al.*, 2016] and selected for O_2 isotopologue composition measurements in duplicate. Flights associated with the campaign took place over the continental United States in August and September of 2013. Samples were selected from five individual flights between 23.7°N and 42.6°N latitude and between 87.3°E and 99.5°E longitude, with potential temperatures ranging from θ = 328 K to θ = 498 K.

Isotopologue ratios of O_2 were measured on a high-resolution Nu Instruments *Perspective IS* isotope ratio mass spectrometer after gas-chromatographic separation from Ar, N_2, and other trace components of air [*Yeung et al.*, 2016; *Yeung et al.*, 2018; *Ash et al.*, 2020]. These ratios are converted to isotopic "delta" notation according to the following definitions:

$$\delta^{18}O = \left(\frac{^{18}\square R_{sample}}{^{18}\square R_{air}} - 1 \right) \delta^{17}O = \left(\frac{^{17}\square R_{sample}}{^{17}\square R_{air}} - 1 \right) \quad (1)$$

$$\Delta_{35} = \left(\frac{^{35}\square R_{sample}}{^{35}\square R_{stochastic}} - 1 \right) \Delta_{36} = \left(\frac{^{36}\square R_{sample}}{^{36}\square R_{stochastic}} - 1 \right) \quad (2)$$

Here, ^{18}R and ^{17}R are the bulk $^{18}O/^{16}O$ and $^{17}O/^{16}O$ ratios in O_2, whereas ^{36}R is the $^{18}O^{18}O/^{16}O^{16}O$ isotopologue ratio. The "stochastic" subscript refers to the random distribution of isotopes within O_2, i.e., $^{35}R_{stochastic} = 2^{17}R_{sample}\,^{18}R_{sample}$ and $^{36}R_{stochastic} = (^{18}R_{sample})^2$. Air sampled from an external staircase on the third floor of the Keith-Wiess Geology building at Rice University several times a week during analytical sessions was used as the bulk-isotope standard against which $\delta^{18}O$ and $\delta^{17}O$ values are reported (i.e., $^{18}R_{air}$ and $^{17}R_{air}$). Reported Δ_{36} values are calibrated against photochemical and heated-gas standards generated at known temperatures according to established techniques [*Yeung et al.*, 2014]. The photochemical standards are generated by submerging a 1 L bulb filled with 1 – 2 mbar of pure O_2 into a constant-

temperature bath held at 22ºC, –25ºC, or –78ºC, allowing the bulb to reach thermal equilibrium, and then photolyzing it with a mercury lamp through an N_2-flushed internal quartz finger for 40 minutes. The effective photolysis temperature reflects the radiative equilibrium between the bath and the finger, which is warmed slightly due to the presence of the lamp and N_2 gas flush (i.e., yielding effective temperatures of 25ºC, –19ºC, or –65ºC for each calibration standard, respectively). High-temperature standards are generated by heating barium peroxide in an evacuated quartz breakseal at 800ºC for 1.5 – 3h, after which the breakseal is quenched by submerging it in room-temperature water.

Samples were analyzed between 2017 and 2019, but only one sample showed a bulk isotopic composition more than 0.1‰ different from air O_2, indicating good isotopic fidelity despite several years' storage. The mean $\delta^{18}O$ deviations from air across the whole dataset were 0.019 ± 0.063‰ (1σ, n = 46 analyses). While omitting the high-$\delta^{18}O$ sample improves the precision across the whole dataset (i.e., $\delta^{18}O$ mean of 0.007 ± 0.036‰), such small positive $\delta^{18}O$ deviations—likely arising from diffusive gas loss rather than a contaminant—are unlikely to affect Δ_{36} values significantly. Therefore, all the SEAC^{4}RS measurements were used. The pooled standard deviation of replicates was ±0.026‰, ±0.071‰ and ±0.045‰ in $\delta^{18}O$, Δ_{35}, and Δ_{36} values, respectively.

2.2 Atmospheric chemical transport modeling

Model simulations using GEOS-Chem (version 12.9.2; http://www.geos-chem.org) and the unified (UCX) chemical mechanism [*Eastham et al.*, 2014] were performed using default global emissions for present-day (PD) simulations of June 1998 – June 2000 and calendar year 2015 [*McDuffie et al.*, 2020]. The UCX mechanism treats stratospheric and tropospheric chemistry under a common scheme and includes explicit accounting of atomic oxygen species, which is necessary for online calculation of Δ_{36} values. The model used meteorology from the Modern Era Retrospective Reanalysis-2 (MERRA2) [*Gelaro et al.*, 2017] with 72 vertical levels (~38 in the troposphere), degraded to a spatial resolution of 4° × 5° (latitude × longitude). Preindustrial era (PI) simulations were also performed using 2015 meteorology with natural (non-anthropogenic) emissions set to those for 1850 C.E. In those simulations, methane, nitrous oxide, and carbonyl sulfide were prescribed using surface mixing ratio boundary conditions that yielded atmospheric concentrations consistent with ice-core constraints [*Murray et al.*, 2014]. Anthropogenic halocarbon concentrations were also prescribed (set to zero) using surface boundary conditions. Biomass burning emissions for the PI are uncertain, with estimates of PI-to-PD changes varying in both sign and magnitude (e.g., PI emissions of 75 – 400% those of the PD) [*McConnell et al.*, 2007; *Marlon et al.*, 2008; *Lamarque et al.*, 2010; *Wang et al.*, 2010; *Bisiaux et al.*, 2012; *Daniau et al.*, 2012; *Pfeiffer et al.*, 2013; *Nicewonger et al.*, 2018; *Dyonisius et al.*, 2020]; recent constraints on PI methane, ethane, and acetylene emissions from biomass burning suggest that they were

comparable to those of the PD, or perhaps slightly higher [*Pfeiffer et al.*, 2013; *Nicewonger et al.*, 2018; *Dyonisius et al.*, 2020; *Nicewonger et al.*, 2020]. Consequently, biomass burning emissions were held constant for PI simulations.

Two online calculation schemes for Δ_{36} values were implemented in GEOS-Chem. Both were simplified schemes designed to minimize the computational burden needed to represent $O(^3P) + O_2$ isotope-exchange chemistry. In the first scheme ("O_2 only"), Δ_{36} values decay toward isotopic equilibrium according to simple first-order kinetics, which are dependent on temperature but independent of O_3 isotopologue chemistry. In the second scheme ("pressure-dependent"), Δ_{36} values decay toward an isotopic steady state rather than isotopic equilibrium. The steady state is determined by local temperature and pressure due to changes in the rates of both isotope-exchange and O_3 isotopologue formation reactions. In both schemes, the temperature, atomic oxygen concentration ($[O(^3P)]$), and O_2 concentration in each grid box determine the local instantaneous rates of isotope exchange. The nominal first-order rate coefficient for the Δ_{36} system was approximated by the temperature-dependent $^{16}O(^3P) + {}^{18}O^{18}O$ isotope-exchange rate coefficient reported by *Fleurat-Lessard et al.* [2003], i.e., $k_{exch}(T)$, which is more precise than that originally reported in *Wiegell et al.* [1997]. At each time-step, the concentration of the Δ_{36} tracer is relaxed toward its local equilibrium or steady-state value according to the isotope-exchange lifetime and the length of the time-step. After the chemistry operation, the Δ_{36} tracer is allowed to advect between grid boxes and mix.

In the O_2-only scheme, the local Δ_{36} value relaxes toward its isotopic equilibrium value, $\Delta_{36,equil}$ (see Text S1 for the formula used). The evolution of local Δ_{36} value from time t_0 to $t_0 + \Delta t$ proceeds according to the equation:

$$\Delta_{36,t_0+\Delta t} = \Delta_{36,t_0} + \left(\Delta_{36,equil} - \Delta_{36,t_0}\right) \times \left(1 - e^{-\Delta t/\tau_{exch}}\right) \quad (3)$$

Here, $\tau_{exch} = 1/(k_{exch}(T)[O(^3P)])$ represents the local Δ_{36} lifetime with respect to isotope exchange. In the pressure-dependent scheme, the local Δ_{36} value relaxes toward the steady-state value $\Delta_{36,ss}$ instead of $\Delta_{36,equil}$, with the other quantities remaining the same. The particular value of $\Delta_{36,ss}$ was determined by polynomial fits to the results of an isotope-enabled photochemical model (i.e., a photochemical kinetics model that includes all isotopologue-specific rate coefficients and species; see Section 2.3).

The online Δ_{36} outputs included full O_2-only and pressure-dependent outputs (herein Δ_{36T} and Δ_{36P}, respectively), as well as diagnostic Δ_{36} values for isotope exchange occurring only within the troposphere (Δ_{36Tt} and Δ_{36Pt}) or only within the stratosphere (Δ_{36Ts} and Δ_{36Ps}). These latter diagnostics were calculated by turning off the operation in eq. 3 if a grid box is above or below the local tropopause, respectively, during

a time-step. The tropopause is determined during each time-step using the World Meteorological Organization lapse-rate definition (i.e., $\Gamma < 2$ K/km).

2.3 Isotope-enabled photochemical model to determine $\Delta_{36,ss}$ values

The 321-reaction KINTECUS photochemical model for the O-O_2-O_3 system from *Yeung et al.* [2014] was updated to include temperature- and pressure-dependent isotope effects for O_3 formation in the atmosphere [*Ianni*, 2003]. Nitrogen (N_2) was added as a separate species to yield near-atmospheric mixing ratios of N_2 and O_2 (i.e., 79% N_2 and 21% O_2); argon was not included for simplicity and because isotope effects in O_3 formation in argon appear to be similar to those of N_2 and O_2 [*Morton et al.*, 1990; *Thiemens and Jackson*, 1990; *Feilberg et al.*, 2013]. The chemistry of nitrogen oxides was omitted because the goal was to simulate the effects of pressure on the O-O_2-O_3 isotopic system only.

The temperature dependencies of ^{18}O-containing O_3 formation rate coefficients were obtained from *Janssen et al.* [2003], while the pressure dependencies for the relative rate coefficients of the $^{16}O + {}^{16}O^{18}O + M \rightarrow {}^{16}O^{16}O^{18}O + M$ and $^{16}O + {}^{18}O^{18}O + M \rightarrow {}^{16}O^{18}O^{18}O + M$ reactions were obtained from *Guenther et al.* [1999]. The temperature and pressure dependencies of these relative rate coefficients were combined using the following expression from *Guenther et al.* [1999] for O_3 isotopologue enrichments:

$$E_{O_3}(T,P) = \frac{E_{O_3}(T)}{1 + P/P_{1/2}} \quad (4)$$

where E_{O3}(T) is the temperature-dependent enrichment of an O_3 isotopologue relative to $^{16}O_3$ at 300K/200 Torr obtained from *Janssen et al.* [2003] [e.g., $E_{O3}(T) = 0.47 + (T - 300\ K) \times 0.00015$ for $^{16}O + {}^{18}O^{18}O$], and $P_{1/2}$ is the pressure at which the enrichment is halved, obtained from *Guenther et al.* [1999] (e.g., $P_{1/2}$ = 4100 Torr or 5466 mbar for $^{16}O + {}^{18}O^{18}O$). The ratio of rate coefficients for the formation of $^{16}O^{16}O^{18}O$ and $^{16}O^{18}O^{18}O$, relative to $^{16}O_3$, is thus $1 + E_{O3}(T,P)$. While the 300K/200 Torr anchor point yields zero-pressure E_{O3} values that differ slightly from those used in *Guenther et al.* [1999], they agree within several percent; the method used here yields slightly better agreement with the measurements reported in *Janssen et al.* [2003]. The ratio of rate coefficients for the $^{18}O + {}^{16}O^{16}O + M \rightarrow {}^{16}O^{16}O^{18}O + M$ and $^{18}O + {}^{18}O^{18}O + M \rightarrow {}^{18}O^{18}O^{18}O + M$ reactions has a negligible dependence on pressure [*Guenther et al.*, 1999], so the 300K/200 Torr relative rate coefficients were used and kept constant [*Mauersberger et al.*, 1999]. The 300K/200 Torr isotopologue-specific relative rate coefficients measured by *Mauersberger et al.* [1999] were also used and held constant wherever temperature- and pressure-dependent data were not available (e.g., for ^{17}O-containing O_3 isotopologues). Because of these missing inputs, Δ_{35} values simulated by this model at elevated pressures are unlikely to be accurate; those results are not reported.

Where possible, the relative rate coefficients for $O(^3P) + O_2$ isotope exchange reactions were determined assuming microscopic reversibility at isotopic equilibrium for each temperature [*Hathorn and Marcus*, 2000; *Wang et al.*, 2004; *Yeung et al.*, 2014], with their absolute rates ultimately tied to the $^{16}O(^3P) + {}^{18}O^{18}O$ isotope-exchange rate constant determined by *Fleurat-Lessard et al.* [2003], i.e., $k_{exch}(T) = 2.7 \pm 0.4 \times 10^{-12}\ (T/300)^{-0.9 \pm 0.5}$ cm^3 s^{-1} (2σ). Seven ^{17}O-containing reactions of the 18 total isotope-exchange reactions were assigned nominal 300 K rate coefficients (i.e., $k_{exch} = 1.5 \times 10^{-12}$ cm^3 s^{-1} per product channel) because their rate coefficients are not known. Previous work has shown that factor-of-two variations in these rate coefficients have a negligible effect on steady-state Δ_{36} values [*Yeung et al.*, 2014].

Isotope effects in other reactions (e.g., during O_3 photolysis or chemical destruction) may also be important, but their cumulative effects on $^{16}O^{18}O$ and $^{18}O^{18}O$-containing species in the atmosphere are poorly known. Owing to the uncertainties in these quantities [*Liang et al.*, 2006; *Früchtl et al.*, 2015a; *Früchtl et al.*, 2015b; *Huang et al.*, 2019], this model only explores the relationship between the isotope effects for $O(^3P) + O_2$ isotope exchange and O_3 formation. We acknowledge that the results obtained are necessarily incomplete, although they are still informative and relevant to the global atmosphere.

Photochemical simulations were performed to generate an array of steady-state solutions between 175 K and 325 K and 0.3 mbar and 4000 mbar total pressure. The relative rates of O_2 and O_3 photolysis were adjusted to yield ~50 ppb O_3 at tropospheric pressures. Each model was run using the mean and 2σ uncertainty bounds for $k_{exch}(T)$. At low temperatures, the uncertainty in $k_{exch}(T)$ is nearly a factor of two (Fig. 1, left), which dominates the overall uncertainty in $\Delta_{36,ss}$ values.

A parameterization for $\Delta_{36,ss}$ as a function of temperature and pressure was made using two polynomial fits. First, third-order polynomial fits for $\Delta_{36,ss}$ vs. pressure were obtained at each temperature (ten different pressures P at each of seven temperatures). The coefficients a, b, c, and d in $\Delta_{36,ss} = aP^3 + bP^2 + cP + d$ were then plotted as a function of temperature, and fifth-order polynomial fits of those trends were obtained. The results are intended for interpolation only under atmospheric conditions (175 – 325 K, 0 – 1100 mbar) given the arbitrary functional form of the fits. The $\Delta_{36,ss}$ value calculated from this two-component scheme was then substituted for $\Delta_{36,equil}$ in eq. 3 to represent the local pressure-dependent Δ_{36} endmember for isotope exchange. This scheme, while simplified, reproduced the $\Delta_{36,ss}$ values in the photochemical model to within 0.01‰. It offers a great reduction in cost compared to representing isotopologue-specific reactions in GEOS-Chem explicitly.

3. Results

3.1 Atmospheric observations of Δ_{36} of O_2

Figure 2 shows the new Δ_{36} measurements on the SEAC^{4}RS samples, which were collected by the NASA ER-2 aircraft, along with previous high-precision measurements made at Rice University on samples from the SOLVE mission (NASA ER-2), the DC3 mission (NASA DC-8), and high-altitude balloon flights over Fort Sumner, NM [*Yeung et al.*, 2016]. The Δ_{36} values from SEAC^{4}RS samples decrease from ~2.7‰ at θ = 500K toward the tropospheric value of 1.99‰, which is reached at θ = 360K and below (Fig. 2A). A maximum value of 2.77‰ was observed in the lower stratosphere at 24°N (θ = 444K). The new data show remarkable consistency with previously reported observations from the midlatitude upper troposphere and stratosphere when plotted against potential temperature [*Yeung et al.*, 2016]. All the SEAC^{4}RS samples below θ = 475 K were analytically more than 2σ different from isotopic equilibrium, with deviations as large as –1.06‰ relative to $\Delta_{36,equil}$ values implied by *in situ* sampling temperatures (Figs. 2B and S1). The largest disequilibria were observed in the tropopause region (e.g., θ = 360K), and were larger at 24°N than at 40°N. Notably, in the midlatitudes between θ = 400K and 500K, measured Δ_{36} values decrease just 0.1‰ with decreasing θ, whereas $\Delta_{36,equil}$ values increase by as much as 0.4‰. The Δ_{36} disequilbrium there thus primarily reflects an increase in $\Delta_{36,equil}$ values. By contrast, the Δ_{36} disequilbrium in the lowermost stratosphere largely reflects the gradient in measured Δ_{36} values rather than the more weakly varying $\Delta_{36,equil}$ values. In the troposphere, the Δ_{36} disequilbrium reflects the homogeneity of Δ_{36} values despite strongly varying temperatures (and therefore also $\Delta_{36,equil}$ values).

Plots of Δ_{36} values versus trace-gas mixing ratios in the same samples show correlations in certain mixing ratio ranges but a limited dependence on latitude in the lower stratosphere (Fig. 2D-F). In particular, Δ_{36} values and O_3 concentrations are positively correlated consistently across multiple field campaigns below 500 ppb O_3. Δ_{36} values and CO concentrations are inversely correlated, whereas Δ_{36} values and CH_4 concentrations are positively correlated below 1700 ppb CH_4 and negatively correlated above. These observations are consistent with high-Δ_{36} stratospheric air mixing with low-Δ_{36} tropospheric air in the lower stratosphere [*Yeung et al.*, 2016]. The change in the relationship between Δ_{36} values and trace gases where O_3 > 500 ppb and CH_4 < 1700 ppb reflects a weak or negligible mixing signal for Δ_{36} values in that region of the stratosphere arising from more rapid photochemical isotope reordering of O_2 [*Yeung et al.*, 2014].

Near 150 ppb O_3—the mixing-ratio-defined tropopause used in some atmospheric chemistry modeling studies (e.g., *Young et al.* [2013])—the SEAC^{4}RS data imply a Δ_{36} value of 2.21 ± 0.04‰ (1σ), which is slightly lower than, but consistent with the previously reported value of 2.32 ± 0.08‰ (1σ) from samples taken from the DC3 campaign [*Barth et al.*, 2015; *Yeung et al.*, 2016]. However, the SEAC^{4}RS data show higher precision and cover both subtropical and extratropical latitudes in the Northern hemisphere. At θ = 380K—the lower bound of the stratospheric "overworld", where isentropic transport does not cross the tropopause, and thus a common isentropic reference surface for computing

stratosphere-to-troposphere mass fluxes [*Holton et al.*, 1995; *Appenzeller et al.*, 1996; *Schoeberl*, 2004]—the SEAC^{4}RS data imply a mean Δ_{36} value of 2.29 ± 0.04‰ (1σ) based on a linear regression of the data between θ = 358 and θ = 406 K (R^2 = 0.96).

3.2 O_2-only online Δ_{36} modeling in GEOS-Chem

Modeled Δ_{36T} values from the O_2-only online calculation agree with measurements for θ > 500 K, but are 0.1‰ – 0.4‰ higher than the measurements below that potential temperature (Fig. 2A). The differences are not due to local meteorological disparities, as agreement between *in situ* and MERRA2 temperatures and pressures is excellent (Fig. S1). At the surface, the simulations yield a global-mean Δ_{36T} value of 2.37‰, whereas measurements consistently yield values that are 0.4‰ lower [*Yeung et al.*, 2014; *Yeung et al.*, 2016; *Li et al.*, 2019; *Yeung et al.*, 2019]. These modeling results are similar to those from the ECHAM/MESSy atmospheric chemistry model [*Gromov et al.*, 2019]. Yet, the qualitative trends seen in the observational dataset are reproduced in the model, with latitude-dependent isotopic disequilibria that are greatest at low latitudes.

The measurement-model disagreement persisted upon variation of many model parameters. For example, altering the rate coefficient for $O(^3P) + O_2$ isotope exchange within the 2σ uncertainty range of laboratory measurements yielded perturbations to the mean surface Δ_{36T} value of <0.01‰. Turning off advective and convective transport changed the surface Δ_{36} value by less than 0.14‰. Resetting Δ_{36T} values of all air parcels that cross the tropopause to a fixed value (values between 1.1‰ and 2.3‰ were evaluated) yielded tropospheric Δ_{36T} values that are within 0.13‰ of that prescribed value.

The diagnostic Δ_{36Tt} and Δ_{36Ts} values—calculated Δ_{36T} values for isotope exchange occurring in the troposphere and stratosphere only—are 2.27‰ and 2.71‰, respectively. The Δ_{36Tt} value corresponds to an effective equilibration temperature of –33°C characteristic of the upper free troposphere. The Δ_{36Ts} value is within 0.1‰ of the simulated Δ_{36} values near the θ = 380K isentrope. Absolute isotope-exchange rates increased by four orders of magnitude from the surface to θ = 900 K, yielding O_2 chemical lifetimes of 0.1 – 1000 days with respect to isotope exchange (Fig. 2C).

3.3. Isotope-enabled photochemical modeling

Incorporation of isotope-specific rate coefficients for O_3 formation into a photochemical model of the O-O_2-O_3-N_2 system, including their pressure- and temperature dependence, revealed deviations from isotopic equilibrium when the system is at photochemical steady state. As pressure increases from 0 to 1500 mbar between 175 K and 325 K, steady-state Δ_{36} values (i.e., $\Delta_{36,ss}$) show deficits relative to $\Delta_{36,equil}$ values (Fig. 3; fit coefficients for $\Delta_{36,ss}$ values are reported in Table S1). The deficits are largest at high pressures, with low-temperature deficits exceeding those at higher temperatures. While the equilibrium

Δ_{36}-temperature relationship is approached in the low-pressure limit, modeled $\Delta_{36,ss}$ values remain 0.01 – 0.04‰ below equilibrium values even at 0.1 mbar. Varying the isotope-exchange rate coefficient $k_{exch}(T)$ about its 2σ uncertainty range changes the magnitude of the $\Delta_{36,ss}$ pressure dependence, with the upper end of the range (i.e., faster rates) yielding smaller steady-state $^{18}O^{18}O$ deficits and vice versa. The resulting uncertainty bounds for $\Delta_{36,ss}$ values at atmospherically relevant conditions are largest at low temperatures and high pressures. For example, at 175 K, the uncertainty in $k_{exch}(T)$ led to an effective 2σ range of 2.3‰ at 1000 mbar (+0.9‰ and –1.4‰ about the mean) but a smaller 2σ range of 0.26‰ at 100 mbar (+0.10‰ and –0.16‰ about the mean). The assumed relative rate of O_3 and O_2 photolysis also affects the magnitude $^{18}O^{18}O$ deficit, but the effect is *O*(0.01‰).

Nulling out the relative rate coefficient enhancements in the $O + O_2 + M \rightarrow O_3 + M$ reactions that form heavy O_3 isotopologues—which are as large as 50% compared to the rate of the $^{16}O_3$-forming reaction—eliminates the pressure-dependent deficits in $^{18}O^{18}O$ relative to isotopic equilibrium when the system is at isotopic steady state. This deviation of $\Delta_{36,ss}$ from $\Delta_{36,equil}$ values is most sensitive to the enhancements in the relative rate coefficients for the $^{16}O + {}^{18}O^{18}O$ and $^{16}O + {}^{16}O^{18}O$ reactions that form O_3. For example, at 1000 mbar and 200 K, the isotope-exchange pathway for $^{16}O + {}^{18}O^{18}O$ collisions outpaces the O_3 production pathway by a factor of ~50. Moreover, a $^{16}O + {}^{18}O^{18}O$ collision produces O_3 ~20% faster than a $^{16}O + {}^{16}O^{18}O$ collision under these conditions [*Guenther et al.*, 1999; *Janssen et al.*, 2003]. This unusually fast transfer of $^{18}O^{18}O$ into O_3, especially compared to $^{16}O^{18}O$, lowers the Δ_{36} value of the remaining O_2 pool. Ozone formation via $^{16}O + {}^{18}O^{18}O$ collisions therefore causes a roughly $1/50 \times 0.2 \times ½ = 2‰$ decrease in Δ_{36} value, comparable to the 1.8‰ difference between $\Delta_{36,equil}$ and $\Delta_{36,ss}$ values obtained from the full photochemical model (note that the factor of ½ arises from the presence of both $^{16}O^{18}O$ and $^{18}O^{16}O$ isotopomers, which halves the effect of the $^{16}O + {}^{18}O^{18}O$ rate enhancement for O_3 formation). A similar calculation at 1000 mbar and 300 K yields an estimated 0.7‰ deficit in $\Delta_{36,ss}$ compared to $\Delta_{36,equil}$, close to the 0.5‰ deficit calculated by the full model. At low pressures, the sequestration of $^{18}O^{18}O$ isotopologues into O_3 is small: $^{16}O + {}^{18}O^{18}O$ isotope exchange is favored by a factor of 10^5 over O_3 formation at 1 mbar and 300 K, resulting in deficits of *O*(0.01‰). These results suggest that the steady-state deficits in $\Delta_{36,ss}$ compared to $\Delta_{36,equil}$ values arise largely from an efficient titration of $^{18}O^{18}O$ by ^{16}O to make excess $^{16}O^{18}O^{18}O$.

We note that the $\Delta_{36,ss}$ values at pressures > 1100 mbar may be most sensitive to uncertainties in the relative temperature- and pressure-dependence of O_3 isotopologue formation rate coefficients; because these pressures are higher than atmospheric pressures, the corresponding $\Delta_{36,ss}$ values are not critical for modeling atmospheric Δ_{36} values, and we do not evaluate them further.

Our preliminary mercury-lamp photolysis experiments, in which air is irradiated for 40 minutes at elevated pressures (500 – 1000 mbar), show large Δ_{36} deficits relative to isotopic equilibrium. An

experiment at 25°C and 887 mbar pressure showed a 0.16‰ deficit, while an experiment at –65°C and 540 mbar showed a 0.9‰ deficit relative to identical experiments performed at < 2 mbar. These experiments confirm the presence of a pressure-dependent photochemical steady state for Δ_{36} values, but the precise Δ_{36} deficits are not yet in quantitative agreement with those predicted by the photochemical model (0.55‰ and 0.95‰, respectively). This disparity may be related to photolytic isotope fractionations for O_3 and O_2 at 254 nm and 185 nm, respectively (i.e., the emission wavelengths of the mercury lamp), which are uncertain for $\delta^{18}O$ and $\delta^{17}O$ and unknown for Δ_{36}. Nevertheless, these experiments are a proof of principle of the $^{18}O^{18}O$ "titration effect," with excellent measurement-model agreement at low temperatures. A thorough laboratory investigation is appropriate for future work.

3.4 Parameterizing the pressure dependence of Δ_{36} values at photochemical steady state

The combined effects of atmospheric pressure and temperature covariations on $\Delta_{36,ss}$ values are shown in Fig. 4 (left panel), along with a comparison with $\Delta_{36,equil}$ values (right panel). Near the surface, the $\Delta_{36,ss}$ value is 0.6‰ to 0.8‰ lower than the $\Delta_{36,equil}$ value and somewhat insensitive to temperature; the pressure dependence largely determines $\Delta_{36,ss}$ values. In the mid- to upper stratosphere, however, $\Delta_{36,ss}$ values are close to $\Delta_{36,equil}$ values, with temperature exerting the dominant control. In between (i.e., the free troposphere up through the lower stratosphere), $\Delta_{36,ss}$ values are consistently lower than $\Delta_{36,equil}$ values, although temperature and pressure are of comparable importance for determining local $\Delta_{36,ss}$ values. These results imply that using $\Delta_{36,ss}$ instead of $\Delta_{36,equil}$ values in atmospheric chemistry simulations will lead to a more pronounced contrast between tropospheric and stratospheric air, and detectable Δ_{36} offsets from the surface to the lower stratosphere.

The results of GEOS-Chem simulations utilizing local $\Delta_{36,ss}$ values are compared to the Δ_{36} observations in Fig. 5. The model for year 2015 shows excellent agreement with the SEAC^{4}RS, DC3, and Ft. Sumner measurements at all altitudes in midlatitudes, with discrepancies smaller than those incurred by the 2σ uncertainty range in the rate coefficient for $O(^3P) + O_2$ isotope exchange. The high-latitude SOLVE samples were obtained in January 2000 from in the polar vortex [*Yeung et al.*, 2009; *Wiegel et al.*, 2013], which can be heterogeneous in space and time; consequently, the 2015 meteorology may not be applicable. The simulations for January 2000, by contrast, explain the SOLVE samples well (Fig. 5, dashed lines). At the surface, the pressure-dependent online Δ_{36} calculation scheme yields a global-mean Δ_{36P} value of 1.97‰ in 2015 with diagnostic Δ_{36Pt} and Δ_{36Ps} values of 1.83‰ and 2.43‰ for troposphere-only and stratosphere-only isotope exchange, respectively (Table 1). The calculated surface Δ_{36P} value is in quantitative agreement with the long-term mean of surface Δ_{36} measurements made at Rice University (1.99 ± 0.02‰; 95% confidence interval), while the Δ_{36Ps} value is ~0.14‰ higher than the Δ_{36} value at the θ = 380 K isentrope implied by the current set of atmospheric observations.

3.5 Modeled spatial and temporal variability in Δ_{36} values

Figure 6 shows modeled seasonal variations in modern-day surface Δ_{36P} values at various sites in the Northern and Southern Hemispheres. Mean Δ_{36P} values are 0.02‰ lower in the Northern Hemisphere, while the seasonal ranges are 0.03‰ and 0.02‰ in the Northern and Southern Hemispheres, respectively. In the O_2-only calculation scheme, the seasonal ranges are slightly smaller (0.02‰ and 0.01‰, respectively). None of these subtle hemispheric differences in Δ_{36} values are currently resolvable using available datasets.

The preindustrial (PI) simulations yielded a global-mean surface Δ_{36P} value that is 0.06‰ higher than the present day (PD) in the pressure-dependent model scheme, whereas it is 0.05‰ higher than the PD in the O_2-only model scheme (Table 1). Moreover, the modeled PI-to-PD Δ_{36} change is insensitive to the 2σ uncertainty range in $\underline{k}_{exch}(T)$: the spread in the PI-to-PD Δ_{36} change is ≤0.004‰ in both online Δ_{36} calculation schemes. Both model schemes therefore yield results that are generally consistent with the PI-to-PD tropospheric Δ_{36} change measured in ice cores (0.03 ± 0.02 decrease; 95% confidence interval) [*Yeung et al.*, 2019], despite measurement-model disagreements in absolute Δ_{36} values. We note that these Δ_{36} differences correspond to the same modeled change in the tropospheric O_3 burden, which is 34% higher in the PD compared to the PI (i.e., 296 Tg O_3 vs. 221 Tg O_3).

4. Discussion

4.1 Assessing the accuracy of the $\Delta_{36,ss}$ pressure dependence

A pressure dependence to $\Delta_{36,ss}$ could have significant implications for interpretating Δ_{36} variations in nature. First, however, one must evaluate whether the pressure-dependent online calculation scheme is accurate by evaluating other potential sources of error. The evidence for an important pressure-dependent effect on atmospheric Δ_{36} values includes: (*i*) observation-model agreement in atmospheric Δ_{36} values above θ = 500 K, but Δ_{36} disagreements below in the O_2-only calculation scheme, (*ii*) demonstrated isotopic disequilibrium caused by nonstatistical removal of O_2 isotopologues during O_3 formation, and (*iii*) excellent observation-model agreement when $\Delta_{36,ss}$ values are used in place of $\Delta_{36,equil}$ values in GEOS-Chem/MERRA2.

While the modern-day atmospheric observations can be explained within the pressure-dependent framework, other factors are still relevant to consider. In particular, measurement errors, errors in stratosphere-to-troposphere transport (STT) in the model, and errors in the rates of oxygen-isotope exchange could be important. We explore each of these possibilities below.

4.1.1 Potential errors in measurements

The agreement between measurements and the GEOS-Chem/MERRA2 model in the middle stratosphere (i.e., 500 K < θ < 950 K), argues against significant measurement errors. The high O(^3P) concentrations in the middle stratosphere—reflected in both the model and prior *in situ* measurements (e.g., ~10^8 cm^{-3} at 30 km in boreal autumn; [*Anderson*, 1975])—yields rapid isotopic reordering in O_2, with O_2 isotope-exchange lifetimes of a day or less [*Yeung et al.*, 2012; *Yeung et al.*, 2014]. Thus, Δ_{36} values are expected to be near local isotopic equilibrium in the middle stratosphere, where $\Delta_{36,ss}$ and $\Delta_{36,equil}$ values are within 0.03‰ of each other. The measurements made at Rice University are consistent with this expectation. Mass-spectrometric scale distortions in Δ_{36} measurements are accounted for by low-pressure (<2 mbar) photochemical and high-temperature calibration experiments performed during every analytical session [*Yeung et al.*, 2014; *Yeung et al.*, 2018]. The associated uncertainties are an order of magnitude smaller than the observation-model disagreements in the lower stratosphere and troposphere. Measured differences in Δ_{36} values between photochemical calibration standards are typically within 0.03‰ of those predicted by theory; these deviations are quantitatively attributable to a combination of isotopic reordering during sample handling [*Yeung et al.*, 2012] and possibly a subtle pressure-dependent effect that is not currently resolvable. Moreover, recent work demonstrating reasonable agreement between first-principles theory and respiratory fractionation of Δ_{36} values [*Ash et al.*, 2020] offers ancillary evidence arguing against large analytical errors (i.e., >0.05‰) in the measurements made at Rice University.

Finally, all Δ_{36} and Δ_{35} values measured at Rice to date covary along a mass-dependent fractionation trend (Fig. 7, which shows the slope of 1.92 for isotopic equilibrium [*Wang et al.*, 2004]). While the exact pressure-dependent relationship between $\Delta_{36,ss}$ and $\Delta_{35,ss}$ values is not independently known, the O_3 formation reactions most relevant to $\Delta_{35,ss}$ values (e.g., $^{16}O + {}^{17}O^{18}O$ and $^{16}O + {}^{16}O^{17}O$) are predicted to have rate coefficients similar to those most relevant to $\Delta_{36,ss}$ values [*Hathorn and Marcus*, 2000]. However, the relative rate coefficients for O(^3P) + O_2 isotope exchange are mass-dependent, so the net titration of $^{17}O^{18}O$ isotopologues is expected to occur in proportion to their steady-state abundances; ozone formation should not strongly alter the relationship between Δ_{36} and Δ_{35} values. Consequently, the measured mass-dependent covariation in Δ_{36} and Δ_{35} values argues against analytical biases in Δ_{36} measurements, but this inference remains to be verified by measurements of isotopologue-specific rate coefficients.

One other laboratory has reported Δ_{36} measurements on air samples from the midlatitude upper troposphere and lower stratosphere. The Δ_{36} values reported in *Laskar et al.* [2019] are all 0.3 – 0.4‰ higher than the Ft. Sumner and SEAC^{4}RS data (samples from September 2004 and 2013, respectively), despite the common latitude range and season (34°N – 42°N, 10 – 20 km, sampled September 2016). Reported Δ_{36} values for surface air from Utrecht, The Netherlands are also higher than the values reported

for surface air in earlier papers [*Yeung et al.*, 2012; *Yeung et al.*, 2014; *Yeung*, 2016; *Li et al.*, 2019]. At face value, the uniformly higher tropospheric and lower-stratospheric Δ_{36} values in *Laskar et al.* [2019] might favor the O_2-only photochemical scheme; however, such a result would imply a profound inaccuracy in the Rice data. Importantly, a large offset in the Rice data would imply that the midlatitude middle stratosphere is far from isotopic equilibrium, contrary to expectations of fast isotopic reordering based on high local $O(^3P)$ concentrations ([*Anderson*, 1975]; see also Fig. 5C). Rapid advection of high-Δ_{36} air from the tropical stratosphere to the midlatitudes could cause a Δ_{36} excess of 0.3 – 0.4‰ in the midlatitude stratosphere (i.e., reflecting air that is 12 – 16°C cooler at equilibrium); however, that air would need to travel at an average speed of ~30 m s^{-1} during the traverse—ten times faster than meridional wind speeds in the MERRA2 reanalysis in the middle stratosphere—without mixing with the surrounding air. We note that the average meridional wind speeds in MERRA2 [$O(1\ m\ s^{-1})$] are consistent with transport timescales from the tropics to the midlatitudes implied by chemical tracer studies [*Boering et al.*, 1996; *Andrews et al.*, 1999]. Furthermore, the narrow spread in measured Δ_{36} values along surfaces of constant potential temperature suggests that dispersive mixing is pervasive and mutes any variability arising from meridional temperature gradients. Consequently, the Δ_{36} values reported in *Laskar et al.* [2019] are incompatible with their atmospheric context. The origin of the interlaboratory disagreement remains unknown, but could plausibly be related to differences in calibration protocols such as the pressures of photolysis of photochemical standards.

4.1.2 Potential errors in stratosphere-troposphere exchange fluxes

Inaccurate STT fluxes could have varied effects on lower-stratospheric Δ_{36} values because O_2 is not at photochemical steady state with respect to its isotopologues. Weak STT fluxes in the model would cause excessive lower-stratospheric residence times, driving Δ_{36} values in the model closer to local $\Delta_{36,equil}$ or $\Delta_{36,ss}$ values than in the observations. STT fluxes that are too strong would have a variety of effects depending on whether the transport is diabatic (e.g., from excessive vertical velocities in the residual circulation) or isentropic (e.g., an excessive diffusive flux). Stronger downward diabatic flow might increase lower-stratospheric Δ_{36} values due to the influx of high-Δ_{36} air from above. This particular case is difficult to distinguish from the weak-STT case, but both scenarios would underestimate the fraction of tropospheric air in the lower stratosphere (i.e., air that has not been photochemically reordered since crossing the tropopause). By contrast, excessive isentropic mixing would increase the fraction of tropospheric air in the lowermost stratosphere, rendering modeled Δ_{36} values there too low.

We therefore used the fraction of tropospheric air as a metric to evaluate the accuracy of STT in the model. A two-component mass balance between tropospheric O_2 and stratospherically reordered O_2 in air for each sample can be constructed to approximate the lower-stratospheric budget:

$$\Delta_{36,\text{observed}} = f_{\text{trop}}\Delta_{36,\text{trop}} + (1 - f_{\text{trop}})\Delta_{36,ss\ or\ equil} \quad (5)$$

Here, stratospheric O_2 is defined as O_2 that was recently reset to its local $\Delta_{36,ss}$ or $\Delta_{36,equil}$ value. An estimate of the fraction of tropospheric air, f_{trop}, can thus be derived from an observed Δ_{36} value and the calculated local $\Delta_{36,ss}$ or $\Delta_{36,equil}$ endmember of the sampling location. While the assumption that only local reordering and mixing alters Δ_{36} values leads to some uncertainties in this estimate for f_{trop}, the results should be sufficient to test for gross errors in STT because the lapse rate is small in the lower stratosphere, resulting in smaller variations in $\Delta_{36,ss}$ or $\Delta_{36,equil}$. We used $\Delta_{36,\text{trop}}$ = 1.99‰ for the measurements [*Yeung et al.*, 2019] and $\Delta_{36,\text{trop}}$ = 1.97‰ (pressure-dependent scheme) or 2.37‰ (O_2-only scheme) for the model to maintain internal consistency.

To facilitate comparison with other studies of STT, the modeled isotope-exchange timescale from GEOS-Chem, τ_{exch}, was used to derive an effective mean residence time ($\tau_{\text{residence}}$) from the equation

$$f_{trop} = e^{-\tau_{residence}/\tau_{exch}} \quad (6).$$

This effective mean residence time can be directly compared to mean residence times for the lowermost stratosphere reported in observational studies. A disagreement between the $\tau_{\text{residence}}$ values obtained via Δ_{36} measurements, the model, and other observational studies would indicate shortcomings in the calculation of the $\Delta_{36,ss}$ endmembers, τ_{exch}, or the two-endmember approach.

Figure 8 shows the values of f_{trop} and $\tau_{\text{residence}}$ derived from this analysis. In both schemes, the tropospheric fraction is less than 5% above θ = 450 K and it increases below, with excellent observation-model agreement. The data also support a subtle meridional trend in modeled f_{trop} values, in which subtropical f_{trop} values are 10 – 15% higher than midlatitude values at the same potential temperature. Calculated residence times range between 20 and 60 days in the lowermost stratosphere (i.e., θ < 380 K), consistent with observationally constrained estimates of 20 – 80 days in the tropical tropopause layer documented during boreal winter [*Andrews et al.*, 1999; *Krüger et al.*, 2009]. STT mass fluxes in the MERRA2 reanalysis therefore appear reasonably accurate, at least for the purposes of this measurement-model comparison.

4.1.3 Potential errors in $O(^3P) + O_2$ isotope-exchange rates

The measurement-model agreement in the O_2-only calculation scheme could potentially be improved if lower-stratospheric $O(^3P) + O_2$ isotope-exchange rates are overestimated and/or tropospheric isotope-exchange rates are underestimated. Because the uncertainty in laboratory measurements of $k_{\text{exch}}(T)$ has only a weak effect on the O_2-only online Δ_{36} results (cf. Fig. 2), the changes in isotope-exchange rates would need to be driven by changes in $O(^3P)$ concentrations. GEOS-Chem's chemical mechanism does

omit $O_2(^1\Sigma)$ chemistry, which can lead to an underestimate of $O(^3P)$ concentrations particularly in the stratosphere [*Yeung et al.*, 2014], but the accuracy of stratospheric O_3 concentrations calculated by the UCX mechanism [*Eastham et al.*, 2014] disfavors this scenario: an additional odd-oxygen source in the stratosphere would increase O_3 concentrations and drive lower-stratospheric Δ_{36} values closer to isotopic equilibrium, exacerbating existing disagreements. Similarly, the high accuracy of tropospheric O_3 concentrations in GEOS-Chem argues against a major (e.g., factor-of-two or more) deficit in tropospheric $O(^3P)$ concentrations at the global scale [*Hu et al.*, 2017].

A preponderance of evidence therefore supports a pervasive titration of $^{18}O^{18}O$ into O_3 in the atmosphere, which results in lower atmospheric Δ_{36} values than isotopic equilibration would predict. Thus, an error in the Rice laboratory measurements does not need to be invoked; the GEOS-Chem/MERRA2 model represents STT and photochemical isotope exchange reasonably well; and uncertainties in the isotope-exchange rates cannot account for the magnitude of the Δ_{36} offsets between measurements and the O_2-only photochemical scheme. Given this evidence, we can now explore the implications this new pressure-dependent isotope chemistry has for our understanding of the global Δ_{36} budget.

4.2 Revisiting the global Δ_{36} budget: reconciling online and offline calculation approaches

4.2.1 Comparing the online and offline (two-box) models

Tropospheric Δ_{36} values are determined largely by the balance of two processes: $O(^3P) + O_2$ reactions and stratosphere-troposphere mass exchange. Model predictions using pressure-dependent $\Delta_{36,ss}$ values affect the implied importance of each process, but not the overall form of the budget. Therefore, in steady state, and omitting biological oxygen cycling (which has a negligible contribution to the global Δ_{36} budget [*Yeung et al.*, 2015]), one can describe the tropospheric budget as a two-endmember mixture:

$$\Delta_{36,trop} \approx \left(\frac{E_{trop}}{F_{ST}+E_{trop}}\right)\Delta_{36,Pequil} + \left(\frac{F_{ST}}{F_{ST}+E_{trop}}\right)\Delta_{36,strat} \quad (7)$$

Here, E_{trop} (mol yr^{-1}) is the effective integrated isotope-exchange flux in the troposphere, F_{ST} (mol yr^{-1}) is the STT flux of O_2, $\Delta_{36,Pequil}$ is the global effective-mean $\Delta_{36,ss}$ value for the troposphere, and $\Delta_{36,strat}$ is the global effective-mean Δ_{36} value of air descending from the stratosphere into the troposphere. Note that the Δ_{36Pt} and Δ_{36Ps} values calculated online in the simulations correspond to $\Delta_{36,Pequil}$ and $\Delta_{36,strat}$ values, respectively.

Previously, the quantities in eq. 7 were determined "offline" using a chemical tropopause (150 ppb O_3), an empirical $\Delta_{36,strat}$ value, and model-derived E_{trop} and $\Delta_{36,Pequil}$ values because online calculations

were not yet available [*Yeung et al.*, 2016; *Yeung et al.*, 2019]. The resulting balance yielded $\Delta_{36,trop}$ values similar to observations. However, the online modeling results reported here suggest that the previous approach was not internally consistent, and thus may be conceptually flawed. For example, using the offline scheme described in *Yeung et al.* [2016], one would derive a $\Delta_{36,Pequil}$ value of 1.45‰ and a $\Delta_{36,trop}$ value of 1.64‰ for the present day, both of which are much lower than the corresponding quantities obtained from the online calculation (Δ_{36Pt} = 1.83‰ and $\Delta_{36,trop}$ = 1.97‰). Thus, it is useful to examine how the online and offline calculations might be reconciled, both to correct any conceptual disparities that may exist and to improve our understanding of the online model results.

First, we will examine how the offline $\Delta_{36,Pequil}$ and online Δ_{36Pt} values can be reconciled. By comparing the $\Delta_{36,Pequil}$ and Δ_{36Pt} values obtained for present-day and preindustrial simulations, we find that online Δ_{36Pt} values are most closely reproduced offline by the weighting scheme below, which is similar to, but slightly different from that used in *Yeung et al.* [2016]:

$$E_{trop} = \frac{\sum_{trop\,grid\,boxes} k_{exch}(T)\left[O\left(^3P\right)\right]\left[O_2\right] m_{box}\,\rho_{box}^{n}}{\sum_{trop\,grid\,boxes} m_{box}\,\rho_{box}^{n}} \times V_{trop} \tag{8}$$

$$\Delta_{36,Pequil} = \frac{\sum_{trop\,grid\,boxes} k_{exch}(T)\left[O\left(^3P\right)\right]\left[O_2\right] m_{box}\,\rho_{box}^{n}\,\Delta_{36,Pequil,box}}{\sum_{trop\,grid\,boxes} k_{exch}(T)\left[O\left(^3P\right)\right]\left[O_2\right] m_{box}\,\rho_{box}^{n}} \tag{9}$$

Each equation represents the annual tropospheric mean obtained by weighting contributions from different processes within each tropospheric grid box. The first term in the numerators of both equations, $k_{exch}(T)[O(^3P)][O_2]$, is the local rate of isotope exchange in units of concentration per unit time; m_{box} is the mass of air used to normalize for the variable size of grid boxes, and V_{trop} is the volume of the troposphere.

The generalized $\rho_{box}{}^{n}$ term differs from that used in *Yeung et al.* [2016], where n was assumed to be unity. Here, the exponent n is introduced to acknowledge that two factors influence the progression of the Δ_{36} value toward $\Delta_{36,ss}$ in each box on longer (e.g., monthly) timescales. The first factor, the cumulative residence time in a grid box, was previously argued to vary proportionately with the number density ρ_{box} (i.e., n = 1) because a well-stirred troposphere should be ergodic: the ensemble mean is equal to the temporal mean. Therefore, higher mean number densities imply longer cumulative residence times for air molecules in those boxes. The second factor affecting the approach of the Δ_{36} value toward $\Delta_{36,ss}$ in each box is the isotope-reordering efficiency. It scales inversely with the number density ρ_{box} (i.e., n = –1)

because isotopic steady state is reached more quickly when fewer O_2 molecules are present—fewer exchange events are required. This second factor was not considered in *Yeung et al.* [2016].

The value of n that reproduces the online Δ_{36Pt} value for 2015 is –0.8, indicating that the isotope-exchange efficiency in each grid box is much more important than the cumulative air parcel residence time for determining tropospheric Δ_{36} values. For example, in the upper troposphere, GEOS-Chem predicts molar isotope-exchange rates that are roughly ten times faster than at the surface ($\tau_{exch} \sim 10^2$ vs. 10^3 days; see Fig. 5C). Number densities are also about tenfold lower in the upper troposphere. Together, these two properties make isotope exchange ~100 times faster in the upper troposphere than at the surface. Atmospheric mixing counteracts the effects of residence-time differences between the lower and upper troposphere, further amplifying the importance of isotope exchange in the upper troposphere. Isotope exchange in the upper troposphere thus appears to be the dominant contribution to the $\Delta_{36,Pequil}$ value. The optimal value of n, however, depends on the balance of chemistry and transport in principle, and thus may be model- and climate-dependent: we find that faster rates of isotope exchange decrease the importance of local residence-time differences (e.g., $n = -1$ was optimal for the $+2\sigma$ simulation) while slower rates of isotope exchange increase their importance (e.g., $n = -0.3$ for the -2σ simulation). Yet, calculated differences in $\Delta_{36,Pequil}$ between preindustrial and present-day scenarios changed <0.002‰ upon varying the value of n between –1 and –0.3.

Using eq. 8 above, one can also evaluate the relative importance of different regions to the present-day $\Delta_{36,Pequil}$ value. The results show that the major contribution to the annual-mean $\Delta_{36,Pequil}$ value comes from the low- and mid-latitude free troposphere in GEOS-Chem/MERRA2 (Fig. 9). Peaks in boreal spring and summer in the extratropics were identified, indicating that both STT of O_3 and anthropogenic emissions influence the seasonal $\Delta_{36,Pequil}$ value by accelerating $O(^3P) + O_2$ isotope exchange reactions locally. Integrated annually and globally, the mean effective altitude for tropospheric photochemistry is 10.1 km, with a broad 1σ-equivalent width of approximately ±4.5 km about the mean. This effective mean altitude is higher than that previously reported (~5 km; [*Yeung et al.*, 2016]) and reflects the greater importance of upper-tropospheric photochemical reordering uncovered in this study. The zonal distribution is similar to that of Earth's surface area, with a maximum in isotope-exchange flux in the relatively cloud-free subtropics (Fig. 9). The tropospheric contribution to the Δ_{36} budget is therefore sensitive to photolysis, chemistry, and temperature of the free troposphere on the global scale.

4.2.2 Revising the terms in the two-box model

We will now compare the online-modeled Δ_{36Ps} value with the empirically determined $\Delta_{36,strat}$ value used in eq. 7. The latter depends strongly on how the tropopause is defined, and its accuracy is limited by the number and spatiotemporal coverage of available observations. Our Northern-Hemisphere observations currently suggest that the $\Delta_{36,strat}$ value is between 2.2 and 2.3‰ when using $\theta = 380$ K or

150 ppb O_3 as the effective Δ_{36} tropopause (Fig. 5D). The Δ_{36Ps} value of 2.43‰ therefore appears to be 0.1 – 0.2‰ higher than the observed $\Delta_{36,strat}$ value (Table 1). Seasonality may be responsible for this apparent disagreement. Within the online model, the annual-mean Δ_{36Ps} value is closest to Δ_{36} values at θ = 380 K during boreal spring, when net STT fluxes are strongest [*Holton et al.*, 1995; *Appenzeller et al.*, 1996]. However, the majority of lower-stratospheric measurements to date were sampled during boreal autumn, when net mass transport moves mass in the opposite direction, i.e., from the troposphere into the stratosphere. One therefore expects the boreal autumn-biased $\Delta_{36,strat}$ values to be lower than the annual-mean Δ_{36Ps} value because the fraction of unaltered tropospheric air (e.g., f_{trop}) is larger in boreal autumn than in spring. The current set of observations therefore provides an incomplete constraint on Δ_{36Ps}. Nevertheless, the observed seasonal bias is consistent with that expected from the seasonality of stratosphere-troposphere exchange; no inconsistencies are evident.

The preceding discussion thus provides a way to obtain the values of the tropospheric terms in the two-box description of the Δ_{36} budget (eq. 7): when $\Delta_{36Pt} = \Delta_{36,Pequil}$, the online and offline descriptions are equivalent, and yields $E_{trop} = 1.4 \times 10^{19}$ mol O_2 yr^{-1}. The Δ_{36Ps} value (2.43‰) and online $\Delta_{36,trop}$ value (Δ_{36P} = 1.97‰) then allow one to solve for F_{ST}, which is inferred to be 4.3×10^{18} mol O_2 yr^{-1}. This F_{ST} value is similar to the net STT flux derived from seasonal diabatic transport across the θ = 380 K surface in the extratropics used in previous studies (i.e., 4.6×10^{18} mol O_2 yr^{-1}; [*Appenzeller et al.*, 1996; *Schoeberl*, 2004]) and is consistent with the 1 – 2-month mean residence time of air in the extratropical lowermost stratosphere (Fig. 8). The present-day Δ_{36} value at the surface is thus comprised of 77% tropospherically reordered air and 23% stratospherically reordered air in steady state.

We note that the MERRA2 STT flux reported in *Boothe and Homeyer* [2017], i.e., $F_{ST,BH} = 1.2 \times 10^{19}$ mol O_2 yr^{-1}, is threefold larger than the estimate above and would result in an inconsistency of ~0.1‰ in $\Delta_{36,trop}$ values, with the box model yielding $\Delta_{36,trop}$ = 2.11‰. This inconsistency arises because the residence-time threshold used for determining "irreversible" STT trajectories in *Boothe and Homeyer* [2017] is much shorter than typical isotope-exchange lifetimes in the lowermost stratosphere (e.g., 4 days vs. 1-2 months). Consequently, the STT mass flux from the analysis of *Boothe and Homeyer* [2017] includes many tropopause-crossing transients that leave Δ_{36} values largely unaltered in an air parcel; the value of F_{ST} relevant for the global Δ_{36} budget should be smaller. *Škerlak et al.* [2014] found that STT fluxes based on trajectory studies scale inversely with the square root of the STT residence-time threshold. That scaling relationship predicts that high-Δ_{36} stratospheric air becomes irreversibly mixed into the troposphere about a month after descending below θ = 380K, i.e., $F_{ST}/F_{ST,BH} \sim (4 \text{ days} / 30 \text{ days})^{1/2}$, consistent with the expected isotope-exchange lifetime at those altitudes.

4.2.3 Summary of revisions to the Δ_{36} budget

In summary, the two-box offline framework for the atmospheric Δ_{36} budget can be reconciled with the online simulations after a more accurate accounting of photochemical reordering in the upper troposphere and the STT flux relevant for the Δ_{36} tracer. This new analysis reveals that the effective mean altitude interrogated by the tropospheric Δ_{36} tracer is 10 km rather than ~5 km, which was previously suggested based on an incomplete accounting of chemistry and transport [*Yeung et al.*, 2016]. The previous approach had underweighted isotope exchange in the upper troposphere because it did not consider the faster approach to isotopic steady state at low O_2 number densities. Importantly, the present consistency between the online and offline approaches allows one to rapidly evaluate the importance of perturbations (e.g., temperature changes) on past tropospheric Δ_{36} values without requiring additional online simulations.

4.3 Changes in the Δ_{36} budget and O_3 since the preindustrial era

Previous work documented a tropospheric Δ_{36} decrease over the twentieth century associated with an increased tropospheric O_3 burden [*Yeung et al.*, 2019]. Online Δ_{36} calculations and diagnostics allow us to analyze the GEOS-Chem/MERRA2 results here in more detail and estimate the magnitude of known systematic uncertainties, facilitating a more quantitative comparison with the atmospheric record.

The PI and PD simulation results can be summarized as follows: the increase in tropospheric O_3 since 1850 CE yields a predicted $\Delta_{36,trop}$ decrease of 0.06‰. The magnitude of the $\Delta_{36,trop}$ decrease is caused by (*i*) the locus of $O(^3P) + O_2$ isotope exchange shifting toward the Northern Hemisphere and lower altitudes (Fig. 10), resulting in the $\Delta_{36,Pequil}$ value decreasing by 0.04‰ (Table 1), and (*ii*) the effective integrated isotope-exchange flux in the troposphere (E_{trop}) increasing by ~30%. These changes also lead to a 0.01‰ increase in the interhemispheric gradient. We note that the uncertainty bounds derived from online simulations run at the 2σ limits for $k_{exch}(T)$ are <0.005‰ for the PI-to-PD shift in Δ_{36P}.

We will now estimate the known systematic uncertainties. First, the modeled changes reflect present-day meteorology and thus omit the ~1°C global warming since 1850 C.E. This warming has two potentially opposing effects on the mean tropospheric Δ_{36} value: to decrease $\Delta_{36,Pequil}$ further and to increase F_{ST}. The two-box framework suggests that a 1°C tropospheric warming would cause an additional 0.01‰ decrease in $\Delta_{36,Pequil}$, if all else is kept unchanged. However, anthropogenic warming is believed to have also accelerated the lower branch of the Brewer-Dobson circulation by ~10%, which would increase F_{ST} [*Lin and Fu*, 2013]. Using the effective present-day F_{ST} of 4.3×10^{18} mol O_2 yr^{-1} across the tropopause and the model-derived quantities $E_{trop} = 1.1 \times 10^{19}$ mol O_2 yr^{-1}, $\Delta_{36,strat} = 2.43$‰, and $\Delta_{36,Pequil} = 1.87$‰ for the PI, we calculate that a 10% smaller STT flux during the PI results in a 0.01‰ smaller PI-PD shift in global-mean tropospheric Δ_{36} value. Consequently, the two opposing effects of the 1°C warming since the preindustrial cancel within the tropospheric Δ_{36} budget.

Second, interannual variability in meteorology can affect both the magnitude of F_{ST} and the effective chemistry/transport balance (i.e., the exponent *n* in eqs. 8 and 9). Our explorations of these effects suggest that interannual variability about long-term means contributes ~0.01‰ uncertainty to the global-mean $\Delta_{36,trop}$ value for a given emissions scenario and climate state. For example, the mean $\Delta_{36P,}$ Δ_{36Pt}, and Δ_{36Ps} values for GEOS-Chem/MERRA2 simulations from June 1998 – June 2000 were all 0.01‰ higher than in 2015 despite comparable global pollutant emissions [*McDuffie et al.*, 2020].

Third, the biomass burning emissions of nitrogen oxides (NO_x) and carbon monoxide (CO) are still uncertain in the preindustrial atmosphere. Recent studies suggesting that preindustrial biomass burning emissions were higher than they are in the present argue that emissions were as much as 40% higher for CO and 20% higher for NO_x [*Rowlinson et al.*, 2020], perhaps due to land-use change [*Pfeiffer et al.*, 2013; *Andela et al.*, 2017; *Hamilton et al.*, 2018]. Such "high-fire" NO_x and CO emissions from biomass during the PI would reduce the PI-to-PD increase in tropospheric O_3 burden from 34% to 15% [*Murray et al.*, 2014]) and thus also mute the change in tropospheric Δ_{36} value. Taking the change in tropospheric O_3 burden as a proxy for E_{trop}, the "high-fire" scenario would reduce the PI-to-PD change in tropospheric Δ_{36} value by 0.01‰.

Finally, the modeled tropospheric Δ_{36} change over the GISP2 (Summit, Greenland) ice coring site is 0.01‰ larger than over the WAIS-D (West Antarctica) ice coring site in both calculation schemes, reflecting a larger O_3 reduction in the Northern hemisphere. However, this small difference would not be detectable by current analytical methods. Nevertheless, averaging measurements from the Northern and Southern hemispheres provides a more robust estimate of the global tropospheric Δ_{36} value and its changes through time.

This explicit quantification of potential systematic uncertainties in the online Δ_{36} calculation suggests that the modeled decrease in tropospheric Δ_{36} since 1850 C.E. is 0.06 ± 0.02‰ (2σ based on uncertainties added in quadrature), consistent with the mean 0.03 ± 0.02‰ decrease (95% confidence interval) observed in the ice-core record [*Yeung et al.*, 2019]. Despite some uncertainty in the modeled absolute Δ_{36} values arising from the isotopic photochemistry of O_3, the associated systematic uncertainties likely do not contribute more than 0.02‰ to modeled changes in tropospheric Δ_{36} value. Preindustrial scenarios invoking higher biomass-burning emissions of NO_x and CO [*Rowlinson et al.*, 2020] would likely yield an estimated $\Delta_{36,trop}$ change closer to the centroid of the observed probability density distribution.

5. Conclusions

The observational, modeling, and experimental evidence presented in this study all suggest that the titration of $^{18}O^{18}O$ into heavy ozone molecules—an atmospheric sink for $^{18}O^{18}O$ that was previously

thought to be negligible—drives Δ_{36} values toward a photochemical steady state that differs from isotopic equilibrium. An online parameterization of this effect within the GEOS-Chem chemical transport model, based on pressure- and temperature-dependent outputs of a detailed isotope-enabled kinetics model, allows GEOS-Chem to reproduce high-precision laboratory measurements on atmospheric samples collected over a range of latitudes, altitudes, seasons, and years. This improved understanding of the factors that affect atmospheric Δ_{36} values, however, results in only minor changes to the predicted evolution in tropospheric Δ_{36} values over the twentieth century in response to the increase in tropospheric O_3; thus, the Δ_{36} tracer remains a constraint on the global preindustrial O_3 burden. Analytical precision in Δ_{36} measurements and uncertainties surrounding preindustrial biomass burning emissions currently dominate the uncertainty in the measurement-model comparison of PI and PD Δ_{36} values, with the PI-PD change in Δ_{36} values consistent with no more than a 30-40% increase in the tropospheric O_3 burden since 1850 C.E.

Furthermore, the online Δ_{36} calculation scheme described herein allows variations in odd-oxygen chemistry and free-tropospheric temperatures—manifesting as changes in tropospheric Δ_{36} values—to be investigated for past climates within chemical-transport and chemistry-climate models. While O_3 photochemistry and climate are linked through biogeochemistry and atmospheric dynamics [*Alexander et al.*, 2003; *Rind et al.*, 2009; *Murray et al.*, 2014; *Geng et al.*, 2017; *Wang et al.*, 2020], Δ_{36} values may nevertheless offer a valuable constraint on the long-term coevolution of atmospheric chemistry and climate.

Acknowledgements

We would like to thank three anonymous reviewers for their prompt and thorough reviews that improved the manuscript. This research was supported by the David & Lucile Packard Foundation Science & Engineering Fellowship to L. Y. Y., National Science Foundation grants AGS-2002422 (to L. Y. Y.) and AGS-2002414 (to L. T. M), and by NASA's Upper Atmosphere Research Program for collection and processing of whole air samples (grants NNX17AE36G to K.A.B. and NNX17AE43G to E.L.A.). Y. Y. was supported by the Pan Family Postdoctoral Fellowship. Saptarshi Chatterjee is acknowledged for his help in setting up GEOS-Chem at Rice University. The color maps used herein are obtained from *Crameri* [2018].

Data Availability

The measured data and model outputs used to support the conclusions can be accessed at https://doi.org/10.5061/dryad.c866t1g6t.

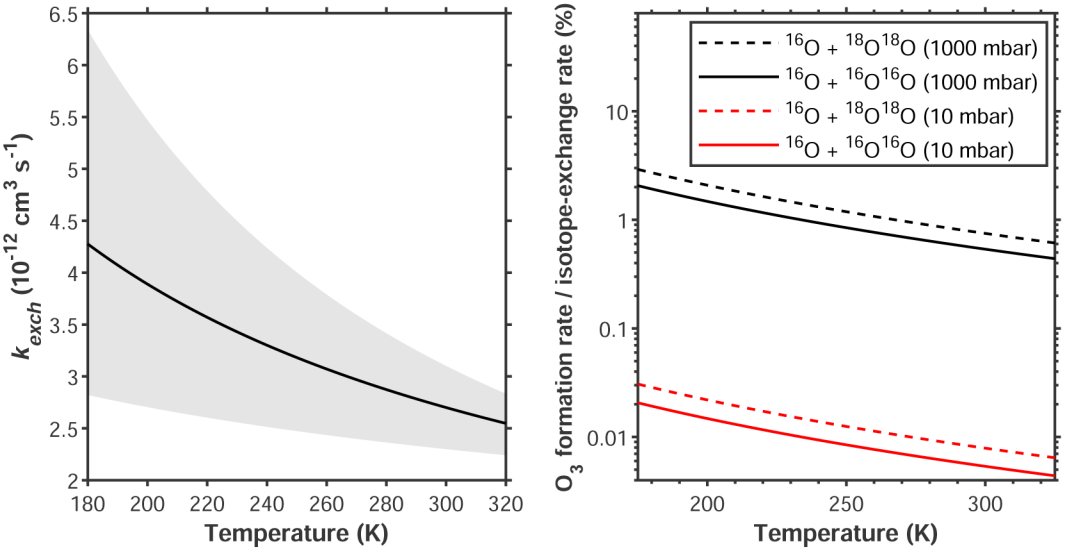

Figure 1. (Left) Temperature dependence of the bimolecular rate coefficient for the $^{16}O + {}^{18}O^{18}O$ isotope-exchange reaction obtained from the combined laboratory/theory study of *Fleurat-Lessard et al.* [2003]. Shaded area represents experimental 2σ uncertainty range. (Right) The ratios of O_3-formation and isotope-exchange rates for $^{16}O + {}^{16}O^{16}O$ and $^{16}O + {}^{18}O^{18}O$ collisions at different pressures, which shows relative rates of O_3 formation that are markedly faster for $^{16}O + {}^{18}O^{18}O$ collisions at high pressures and low temperatures.

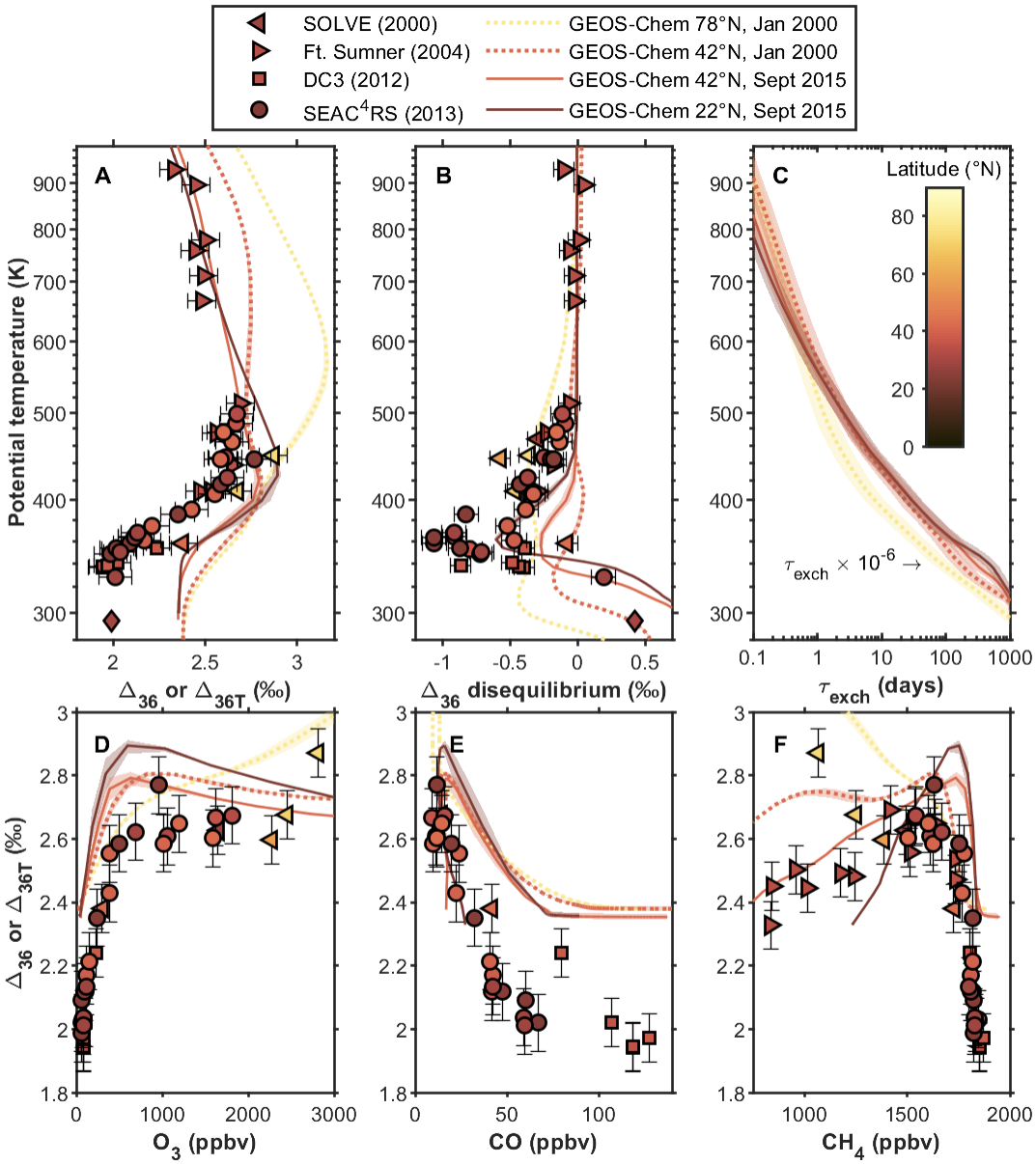

Figure 2. Measurement-model comparison for the O_2-only online Δ_{36} calculation scheme in GEOS-Chem. The diamond in panels A and B reflect the mean surface Δ_{36} value measured in Houston, TX. Error bars on the data points represent the 1σ pooled standard deviation of duplicates. Modeled monthly means from January 2000 and September 2015 are plotted for comparison. Shaded areas represent pseudo-2σ uncertainty bounds obtained by running identical simulations at the experimental ±2σ bounds for k_{exch}(T). Note that the isotope-exchange lifetime for the 78°N, January 2000 profile in panel C is scaled by 10^{-6} for clarity.

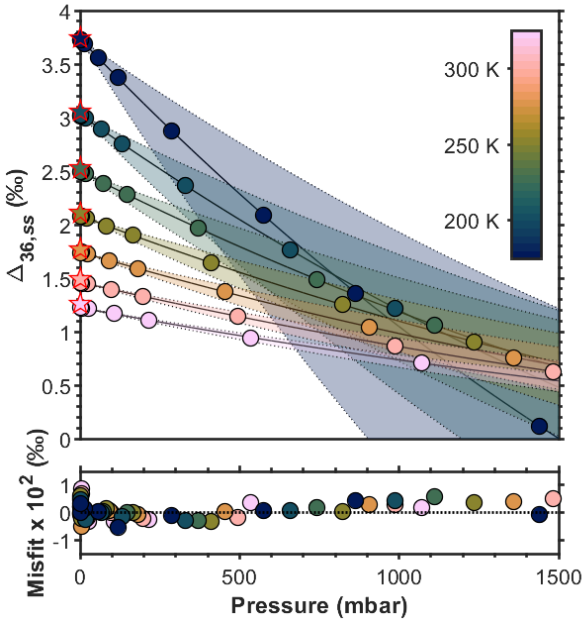

Figure 3. $\Delta_{36,ss}$ vs. pressure from the isotope-enabled photochemical kinetics model for a range of temperatures (filled circles) compared to polynomial fits of the trends (curves). For reference, Δ_{36} values for isotopic equilibrium (i.e., $\Delta_{36,equil}$) are shown as stars on the left axis. Deviations of $\Delta_{36,ss}$ from $\Delta_{36,equil}$ values at 0.1 mbar range from –0.01‰ at 175K to –0.04‰ at 300K**.** The lower plot shows the misfit between the modeled $\Delta_{36,ss}$ compositions and polynomial fits to those values.

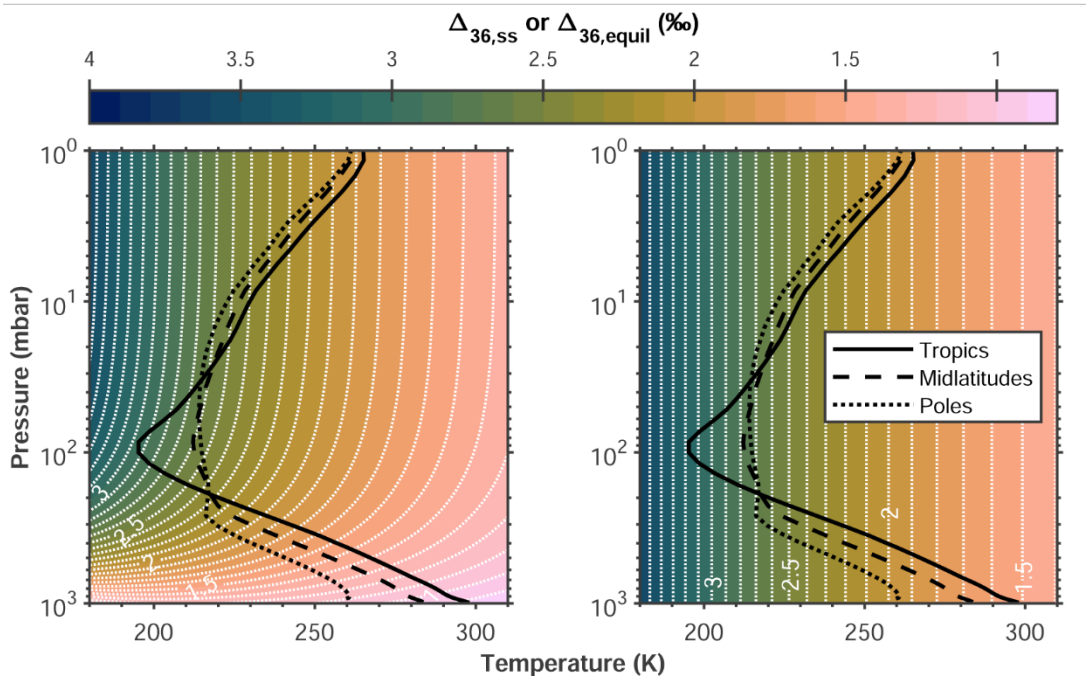

Figure 4. Patterns in $\Delta_{36,ss}$ (left) and $\Delta_{36,equil}$ (right) along atmospheric covariations of temperatures and pressures. Modern annual-mean atmospheric temperature profiles for tropical (30°S – 30°N), midlatitude (30°S – 60°S and 30°N – 60°N), and polar (60°S – 90°S and 60°N – 90°N) latitudes from the MERRA2 reanalysis are overlain.

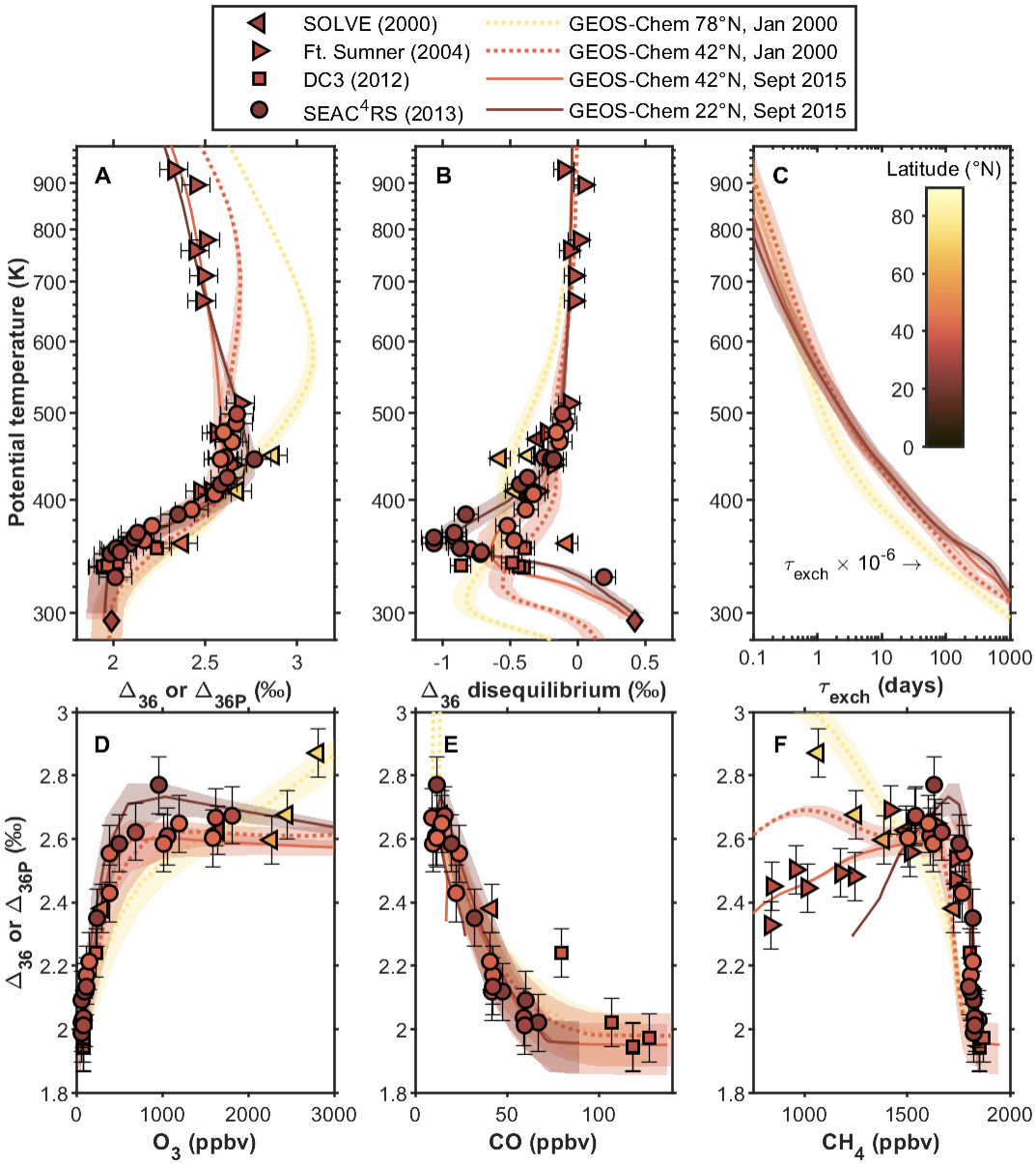

Figure 5. Measurement-model comparison for the pressure-dependent online Δ_{36} calculation scheme in GEOS-Chem. The diamond in panels A and B reflect the mean surface Δ_{36} value measured in Houston, TX. Error bars on the data points represent the 1σ pooled standard deviation of duplicates. Modeled monthly means from January 2000 and September 2015 are plotted for comparison. Shaded areas represent pseudo-2σ uncertainty bounds obtained by running identical simulations at the experimental ±2σ bounds for k_{exch}(T). Note that the isotope-exchange lifetime for the 78°N, January 2000 profile in panel C is scaled by 10^{-6} for clarity.

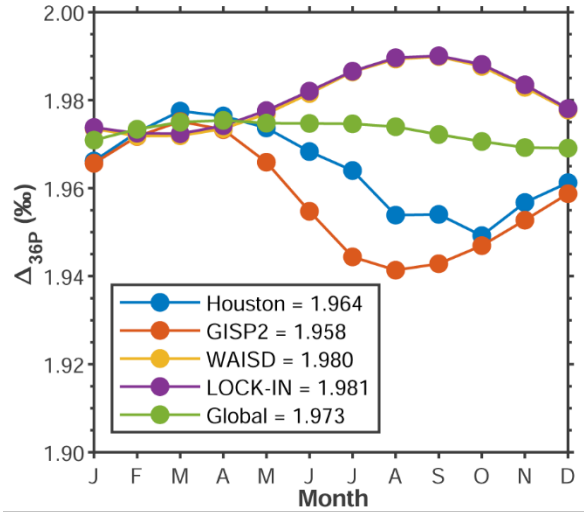

Figure 6. Modeled seasonal cycle of surface Δ_{36P} values at various sites in 2015. The modeled global-mean surface Δ_{36P} value is also shown. Ice-coring site locations are Summit, Greenland (GISP2; 72.6ºN, 38.5 ºW), the West Antarctic Ice Sheet Divide (WAISD; 79.5ºS, 112.1ºW) and East Antarctica near Dome C (LOCK-IN; 74.1ºS, 126.2ºE).

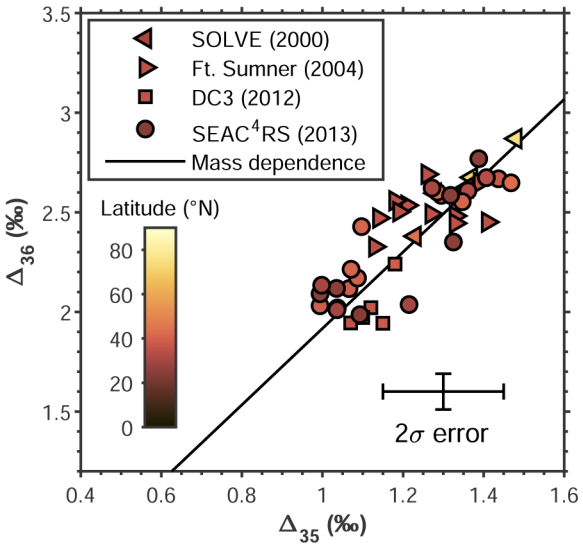

Figure 7. Comparison of Δ_{36} and Δ_{35} values measured on the same samples, which show a mass-dependent trend.

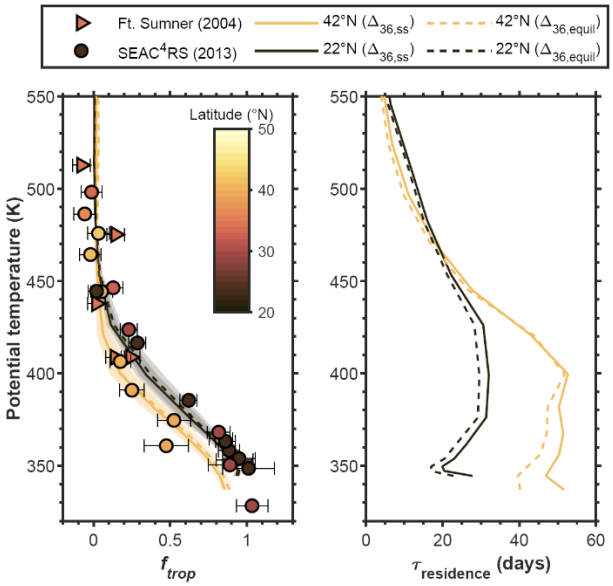

Figure 8. Measurement-model comparison of stratosphere-troposphere mixing fractions (left) and implied lower-stratospheric residence times (right).

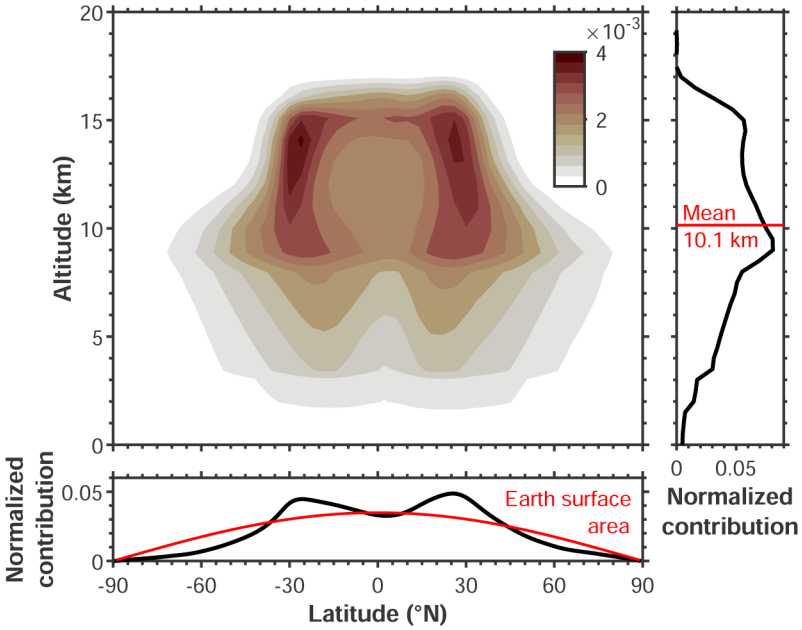

Figure 9. Normalized contour plot depicting where $O(^3P) + O_2$ isotope-exchange chemistry records tropospheric climate (i.e., Δ_{36Pt} or $\Delta_{36,Pequil}$; cf. eq. 7) in GEOS-Chem/MERRA2 model year 2015. Also shown are the integrated normalized contributions as a function of altitude and latitude (black curves). The mean effective altitude (red line in right panel) and Earth surface area (red curve) are shown for comparison.

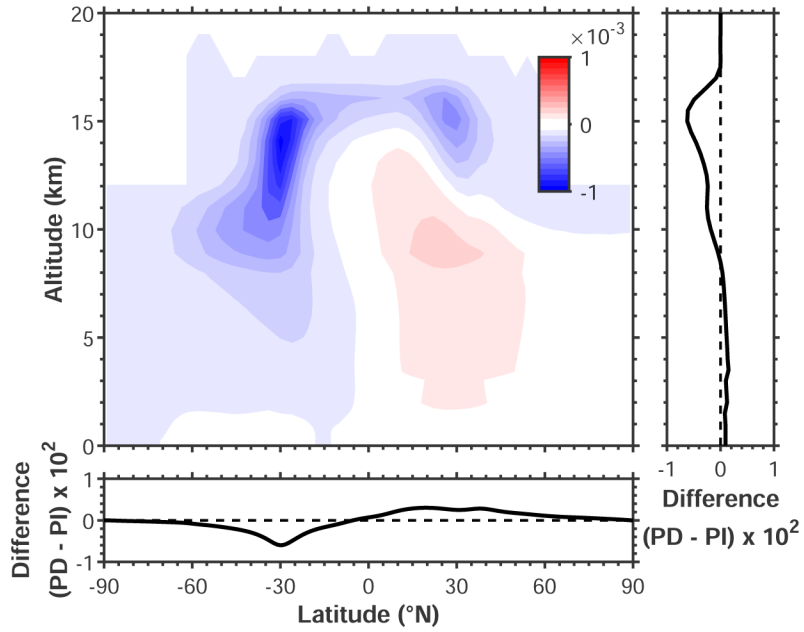

Figure 10. Changes in tropospheric isotope-exchange chemistry from preindustrial to present in GEOS-Chem/MERRA2. Changes are computed as the difference in normalized contribution to the Δ_{36Pt} or $\Delta_{36,Pequil}$ value (e.g., Fig. 9) in each scenario. Positive values indicate increased importance in the present day (PD), while negative values indicate decreased importance, relative to the preindustrial (PI).

Table 1. Comparison of the simulated preindustrial-to-present change in Δ_{36} values and diagnostics using the O_2-only and pressure-dependent calculation schemes.

	O_2-only			Pressure-dependent		
	Δ_{36T} / ‰[*]	Δ_{36Tt} / ‰[†]	Δ_{36Ts} / ‰[‡]	Δ_{36P} / ‰[*]	Δ_{36Pt} / ‰[†]	Δ_{36Ps} / ‰[‡]
Using the mean value for $O(^3P) + O_2$ isotope-exchange rate coefficients, $k_{exch}(T)$[§]						
2015	2.372	2.271	2.712	1.973	1.832	2.430
1850	2.418	2.302	2.710	2.033	1.871	2.428
Change	*-0.046*	*-0.031*	*0.002*	*-0.060*	*-0.039*	*0.002*
Using the lower bound for isotope-exchange rate coefficients, $k_{exch}(T) - 2\sigma$[§]						
2015	2.379	2.253	2.712	1.874	1.691	2.346
1850	2.427	2.283	2.710	1.939	1.730	2.344
Change	*-0.048*	*-0.030*	*0.002*	*-0.065*	*-0.039*	*0.002*
Using the upper bound for isotope-exchange rate coefficients, $k_{exch}(T) + 2\sigma$[§]						
2015	2.367	2.286	2.712	2.042	1.934	2.489
1850	2.411	2.318	2.710	2.100	1.973	2.488
Change	*-0.044*	*-0.032*	*0.002*	*-0.058*	*-0.039*	*0.001*

[*]Simulated global-mean value at the surface
[†]Diagnostic signature for isotope exchange occurring in the troposphere
[‡]Diagnostic signature for isotope exchange occurring in the stratosphere
[§]Mean and uncertainty bounds as reported in *Fleurat-Lessard et al.* (2003).

References

Alexander, B., M. G. Hastings, D. J. Allman, J. Dachs, J. A. Thornton, and S. A. Kunasek (2009), Quantifying atmospheric nitrate formation pathways based on a global model of the oxygen isotope composition ($\Delta^{17}O$) of atmospheric nitrate, *Atmos. Chem. Phys.*, *9*, 5043-5056.

Alexander, B., and L. J. Mickley (2015), Paleo-Perspectives on Potential Future Changes in the Oxidative Capacity of the Atmosphere Due to Climate Change and Anthropogenic Emissions, *Curr. Pollution Rep.*, 1-13, doi:10.1007/s40726-015-0006-0.

Alexander, B., M. H. Thiemens, J. Farquhar, A. J. Kaufman, J. Savarino, and R. J. Delmas (2003), East Antarctic ice core sulfur isotope measurements over a complete glacial-interglacial cycle, *J. Geophys. Res.*, *108*(D24), 4786.

Andela, N., D. C. Morton, L. Giglio, Y. Chen, G. R. van der Werf, P. S. Kasibhatla, R. S. DeFries, G. J. Collatz, S. Hantson, S. Kloster, D. Bachelet, M. Forrest, G. Lasslop, F. Li, S. Mangeon, J. R. Melton, C. Yue, and J. T. Randerson (2017), A human-driven decline in global burned area, *Science*, *356*(6345), 1356-1362, doi:10.1126/science.aal4108.

Anderson, J. G. (1975), The absolute concentration of $O(^3P)$ in Earth's stratosphere, *Geophys. Res. Lett.*, *2*(6), 231-234.

Andrews, A. E., K. A. Boering, B. C. Daube, S. C. Wofsy, E. J. Hintsa, E. M. Weinstock, and T. P. Bui (1999), Empirical age spectra for the lower tropical stratosphere from in situ observations of CO2: Implications for stratospheric transport, *J. Geophys. Res.-Atmos.*, *104*(D21), 26581-26595, doi:https://doi.org/10.1029/1999JD900150.

Appenzeller, C., J. R. Holton, and K. H. Rosenlof (1996), Seasonal variation of mass transport across the tropopause, *J. Geophys. Res.*, *101*(D10), 15071-15078.

Ash, J. L., L. Y. Yeung, and H. Hu (2020), What fractionates oxygen isotopes during respiration? Insights from multiple isotopologue measurements and theory, *ACS Earth and Space Chemistry*, *4*, 50-66, doi:10.1021/acsearthspacechem.9b00230.

Barth, M. C., C. A. Cantrell, W. H. Brune, S. A. Rutledge, J. H. Crawford, H. Huntreiser, L. D. Carey, D. McGorman, M. Weisman, K. E. Pickering, E. Bruning, B. Anderson, E. Apel, M. Biggerstaff, T. Campos, P. Campuzano-Jost, R. Cohen, J. Crounse, D. A. Day, G. Diskin, F. Flocke, A. Fried, B. Heikes, S. Honomichl, R. Hornbrook, L. G. Huey, J. L. Jimenez, T. Lang, M. Lichtenstern, T. Mikoviny, B. Nault, D. O'Sullivan, L. L. Pan, J. Peischl, I. Pollack, D. Richter, D. Riemer, T. Ryerson, H. Schlager, J. St. Clair, J. Walega, P. Weibring, A. Weinheimer, P. Wennberg, A. Wisthaler, P. J. Wooldridge, and C. Ziegler (2015), The Deep Convective Clouds and Chemistry (DC3) Field Campaign, *Bull. Amer. Meteorol. Soc.*, *96*, 1281-1309, doi:10.1175/BAMS-D-13-00290.1.

Bisiaux, M. M., R. Edwards, J. R. McConnell, M. A. J. Curran, T. D. Van Ommen, A. M. Smith, T. A. Neumann, D. R. Pasteris, J. E. Penner, and K. Taylor (2012), Changes in black carbon deposition to Antarctica from two high-resolution ice core records, 1850–2000 AD, *Atmos. Chem. Phys.*, *12*(9), 4107-4115, doi:10.5194/acp-12-4107-2012.

Boering, K. A., S. C. Wofsy, B. C. Daube, H. R. Schneider, M. Loewenstein, J. R. Podolske, and T. J. Conway (1996), Stratospheric mean ages and transport rates from observations of carbon dioxide and nitrous oxide, *Science*, *274*(5291), 1340-1343.

Boothe, A. C., and C. R. Homeyer (2017), Global large-scale stratosphere–troposphere exchange in modern reanalyses, *Atmos. Chem. Phys.*, *17*(9), 5537-5559, doi:10.5194/acp-17-5537-2017.

Crameri, F. (2018), Scientific colour maps, edited, Zenodo, doi:10.5281/zenodo.1243862.

Daniau, A.-L., P. J. Bartlein, S. P. Harrison, I. C. Prentice, S. Brewer, P. Friedlingstein, T. I. Harrison-Prentice, J. Inoue, K. Izumi, J. R. Marlon, S. Mooney, M. J. Power, J. Stevenson, W. Tinner, M. Andrič, J. Atanassova, H. Behling, M. Black, O. Blarquez, K. J. Brown, C. Carcaillet, E. A. Colhoun, D. Colombaroli, B. A. S. Davis, D. D'Costa, J. Dodson, L. Dupont, Z. Eshetu, D. G. Gavin, A. Genries, S. Haberle, D. J. Hallett, G. Hope, S. P. Horn, T. G. Kassa, F. Katamura, L. M. Kennedy, P. Kershaw, S. Krivonogov, C. Long, D. Magri, E. Marinova, G. M. McKenzie, P. I. Moreno, P. Moss,

F. H. Neumann, E. Norström, C. Paitre, D. Rius, N. Roberts, G. S. Robinson, N. Sasaki, L. Scott, H. Takahara, V. Terwilliger, F. Thevenon, R. Turner, V. G. Valsecchi, B. Vannière, M. Walsh, N. Williams, and Y. Zhang (2012), Predictability of biomass burning in response to climate changes, *Global Biogeochem. Cycles*, *26*(4), doi:https://doi.org/10.1029/2011GB004249.

Dyonisius, M. N., V. V. Petrenko, A. M. Smith, Q. Hua, B. Yang, J. Schmitt, J. Beck, B. Seth, M. Bock, B. Hmiel, I. Vimont, J. A. Menking, S. A. Shackleton, D. Baggenstos, T. K. Bauska, R. H. Rhodes, P. Sperlich, R. Beaudette, C. Harth, M. Kalk, E. J. Brook, H. Fischer, J. P. Severinghaus, and R. F. Weiss (2020), Old carbon reservoirs were not important in the deglacial methane budget, *Science*, *367*(6480), 907-910, doi:10.1126/science.aax0504.

Eastham, S. D., D. K. Weisenstein, and S. R. H. Barrett (2014), Development and evaluation of the unified tropospheric–stratospheric chemistry extension (UCX) for the global chemistry-transport model GEOS-Chem, *Atmos. Environ.*, *89*(0), 52-63, doi:10.1016/j.atmosenv.2014.02.001.

Feilberg, K. L., A. A. Wiegel, and K. A. Boering (2013), Probing the unusual isotope effects in ozone formation: Bath gas and pressure dependence of the non-mass-dependent isotope enrichments in ozone, *Chem. Phys. Lett.*, *556*, 1-8, doi:https://doi.org/10.1016/j.cplett.2012.10.038.

Fleurat-Lessard, P., S. Y. Grebenshchikov, R. Schinke, C. Janssen, and D. Krankowsky (2003), Isotope dependence of the O + O_2 exchange reaction: Experiment and theory, *J. Chem. Phys.*, *119*(9), 4700-4712.

Frey, M. M., R. C. Bales, and J. R. McConnell (2006), Climate sensitivity of the century-scale hydrogen peroxide (H2O2) record preserved in 23 ice cores from West Antarctica, *J. Geophys. Res.-Atmos.*, *111*(D21), doi:https://doi.org/10.1029/2005JD006816.

Frey, M. M., J. Savarino, S. Morin, J. Erbland, and J. M. F. Martins (2009), Photolysis imprint in the nitrate stable isotope signal in snow and atmosphere of East Antarctica and implications for reactive nitrogen cycling, *Atmos. Chem. Phys.*, *9*(22), 8681-8696, doi:10.5194/acp-9-8681-2009.

Früchtl, M., C. Janssen, and T. Röckmann (2015a), Experimental study on isotope fractionation effects in visible photolysis of O_3 and in the O + O_3 odd oxygen sink reaction, *J. Geophys. Res.-Atmos.*, *120*(9), 4398-4416, doi:https://doi.org/10.1002/2014JD022944.

Früchtl, M., C. Janssen, D. Taraborrelli, S. Gromov, and T. Röckmann (2015b), Wavelength-dependent isotope fractionation in visible light O3 photolysis and atmospheric implications, *Geophys. Res. Lett.*, *42*(20), 8711-8718, doi:https://doi.org/10.1002/2015GL066219.

Gao, Y. Q., and R. A. Marcus (2001), Strange and Unconventional Isotope Effects in Ozone Formation, *Science*, *293*, 259-263.

Gelaro, R., W. McCarty, M. J. Suárez, R. Todling, A. Molod, L. Takacs, C. A. Randles, A. Darmenov, M. G. Bosilovich, R. Reichle, K. Wargan, L. Coy, R. Cullather, C. Draper, S. Akella, V. Buchard, A. Conaty, A. M. da Silva, W. Gu, G.-K. Kim, R. Koster, R. Lucchesi, D. Merkova, J. E. Nielsen, G. Partyka, S. Pawson, W. Putman, M. Rienecker, S. D. Schubert, M. Sienkiewicz, and B. Zhao (2017), The Modern-Era Retrospective Analysis for Research and Applications, Version 2 (MERRA-2), *J. Clim.*, *30*(14), 5419-5454, doi:10.1175/JCLI-D-16-0758.1.

Geng, L., B. Alexander, J. Cole-Dai, E. J. Steig, J. Savarino, E. D. Sofen, and A. J. Schauer (2014), Nitrogen isotopes in ice core nitrate linked to anthropogenic atmospheric acidity change, *Proc. Natl. Acad. Sci. U. S. A.*, *111*(16), doi:10.1073/pnas.1319441111.

Geng, L., L. T. Murray, L. J. Mickley, P. Lin, Q. Fu, A. J. Schauer, and B. Alexander (2017), Isotopic evidence of multiple controls on atmospheric oxidants over climate transitions, *Nature*, *546*(7656), 133-136, doi:10.1038/nature22340.

Gromov, S., T. Röckmann, A. H. Laskar, and R. Peethambaran (2019), Modelling the abundance of $^{18}O^{18}O$ in the atmosphere and its sensitivity to temperature and O_3 photochemistry, *Geophysical Research Abstracts*, *21*, EGU2019-16938-16931.

Guenther, J., B. Erbacher, D. Krankowsky, and K. Mauersberger (1999), Pressure dependence of two relative ozone formation rate coefficients, *Chem. Phys. Lett.*, *306*(5), 209-213, doi:https://doi.org/10.1016/S0009-2614(99)00469-8.

Hamilton, D. S., S. Hantson, C. E. Scott, J. O. Kaplan, K. J. Pringle, L. P. Nieradzik, A. Rap, G. A. Folberth, D. V. Spracklen, and K. S. Carslaw (2018), Reassessment of pre-industrial fire emissions strongly affects anthropogenic aerosol forcing, *Nat. Commun.*, *9*(1), 3182, doi:10.1038/s41467-018-05592-9.

Hastings, M. G., J. C. Jarvis, and E. J. Steig (2009), Anthropogenic impacts on nitrogen isotopes of ice-core nitrate, *Science*, *324*, 1288.

Hathorn, B. C., and R. A. Marcus (2000), An intramolecular theory of the mass-independent isotope effect for ozone. II. Numerical implementation at low pressures using a loose transition state, *J. Chem. Phys.*, *113*(21), 9497-9509.

Heidenreich, J. E., and M. H. Thiemens (1983), A non-mass-dependent isotope effect in the production of ozone from molecular oxygen, *J. Chem. Phys.*, *78*, 892-895.

Holton, J. R., P. H. Haynes, M. E. McIntyre, A. R. Douglass, R. B. Rood, and L. Pfister (1995), Stratosphere-troposphere exchange, *Rev. Geophys.*, *33*(4), 403-439.

Hu, L., D. J. Jacob, X. Liu, Y. Zhang, L. Zhang, P. S. Kim, M. P. Sulprizio, and R. M. Yantosca (2017), Global budget of tropospheric ozone: Evaluating recent model advances with satellite (OMI), aircraft (IAGOS), and ozonesonde observations, *Atmos. Environ.*, *167*, 323-334, doi:https://doi.org/10.1016/j.atmosenv.2017.08.036.

Huang, C.-H., S. K. Bhattacharya, Z.-M. Hsieh, Y.-J. Chen, T.-S. Yih, and M.-C. Liang (2019), Isotopic Fractionation in Photolysis of Ozone in the Hartley and Chappuis Bands, *Earth and Space Science*, *6*(5), 752-773, doi:https://doi.org/10.1029/2018EA000517.

Ianni, J. C. (2003), A comparison of the Bader-Deuflhard and the Cash-Karp Runge-Kutta integrators for the Gri-Mech 3.0 model based on the chemical kinetics code Kintecus, in *Computational Fluid and Solid Mechanics 2003*, edited by K. J. Bathe, Elsevier Science, Ltd., Oxford.

Janssen, C., J. Guenther, D. Krankowsky, and K. Mauersberger (2003), Temperature dependence of ozone rate coefficients and isotopologue fractionation in ^{16}O–^{18}O oxygen mixtures, *Chem. Phys. Lett.*, *367*, 34-38.

Krüger, K., S. Tegtmeier, and M. Rex (2009), Variability of residence time in the Tropical Tropopause Layer during Northern Hemisphere winter, *Atmos. Chem. Phys.*, *9*(18), 6717-6725, doi:10.5194/acp-9-6717-2009.

Kunasek, S. A., B. Alexander, E. J. Steig, E. D. Sofen, T. L. Jackson, M. H. Thiemens, J. R. McConnell, D. J. Gleason, and H. M. Amos (2010), Sulfate sources and oxidation chemistry over the past 230 years from sulfur and oxygen isotopes of sulfate in a West Antarctic ice core, *J. Geophys. Res.*, *115*, D18313, doi:10.1029/2010JD013846.

Lamarque, J. F., T. C. Bond, V. Eyring, C. Granier, A. Heil, Z. Klimont, D. Lee, C. Liousse, A. Mieville, B. Owen, M. G. Schultz, D. Shindell, S. J. Smith, E. Stehfest, J. Van Aardenne, O. R. Cooper, M. Kainuma, N. Mahowald, J. R. McConnell, V. Naik, K. Riahi, and D. P. van Vuuren (2010), Historical (1850–2000) gridded anthropogenic and biomass burning emissions of reactive gases and aerosols: methodology and application, *Atmos. Chem. Phys.*, *10*(15), 7017-7039, doi:10.5194/acp-10-7017-2010.

Laskar, A. H., R. Peethambaran, G. A. Adnew, and T. Röckmann (2019), Measurement of $^{18}O^{18}O$ and $^{17}O^{18}O$ in atmospheric O_2 using the 253 Ultra mass spectrometer and applications to stratospheric and tropospheric air samples, *Rapid Commun. Mass Spectrom.*, *33*(11), 981-994, doi:10.1002/rcm.8434.

Li, B., L. Y. Yeung, H. Hu, and J. L. Ash (2019), Kinetic and equilibrium fractionation of O_2 isotopologues during air-water gas transfer and implications for tracing biological oxygen cycling in the ocean, *Mar. Chem.*, *210*, 61-71, doi:10.1016/j.marchem.2019.02.006.

Liang, M.-C., F. W. Irion, J. D. Weibel, C. E. Miller, G. A. Blake, and Y. L. Yung (2006), Isotopic composition of stratospheric ozone, *J. Geophys. Res.*, *111*, D02302.

Lin, P., and Q. Fu (2013), Changes in various branches of the Brewer–Dobson circulation from an ensemble of chemistry climate models, *J. Geophys. Res.-Atmos.*, *118*(1), 73-84, doi:10.1029/2012JD018813.

Loomis, S. E., J. M. Russell, D. Verschuren, C. Morrill, G. De Cort, J. S. Sinninghe Damsté, D. Olago, H. Eggermont, F. A. Street-Perrott, and M. A. Kelly (2017), The tropical lapse rate steepened during the Last Glacial Maximum, *Sci. Adv.*, *3*(1), doi:10.1126/sciadv.1600815.

Lueb, R. A., D. H. Ehhalt, and L. E. Heidt (1975), Balloon-borne low temperature air sampler, *Rev. Sci. Instrum.*, *46*(6), 702-705.

Marlon, J. R., P. J. Bartlein, C. Carcaillet, D. G. Gavin, S. P. Harrison, P. E. Higuera, F. Joos, M. J. Power, and I. C. Prentice (2008), Climate and human influences on global biomass burning over the past two millennia, *Nat. Geosci.*, *1*(10), 697-702, doi:10.1038/ngeo313.

Mauersberger, K. (1981), Measurement of heavy ozone in the stratosphere, *Geophys. Res. Lett.*, *8*(8), 935-937.

Mauersberger, K., B. Erbacher, D. Krankowsky, J. Günther, and R. Nickel (1999), Ozone Isotope Enrichment: Isotopomer-Specific Rate Coefficients, *Science*, *283*, 370-372.

McConnell, J. R., R. Edwards, G. L. Kok, M. G. Flanner, C. S. Zender, E. S. Saltzman, J. R. Banta, D. R. Pasteris, M. M. Carter, and J. D. W. Kahl (2007), 20th-Century Industrial Black Carbon Emissions Altered Arctic Climate Forcing, *Science*, *317*(5843), 1381-1384, doi:10.1126/science.1144856.

McDuffie, E. E., S. J. Smith, P. O'Rourke, K. Tibrewal, C. Venkataraman, E. A. Marais, B. Zheng, M. Crippa, M. Brauer, and R. V. Martin (2020), A global anthropogenic emission inventory of atmospheric pollutants from sector- and fuel-specific sources (1970–2017): an application of the Community Emissions Data System (CEDS), *Earth Syst. Sci. Data*, *12*(4), 3413-3442, doi:10.5194/essd-12-3413-2020.

Ming, A., V. H. L. Winton, J. Keeble, N. L. Abraham, M. C. Dalvi, P. Griffiths, N. Caillon, A. E. Jones, R. Mulvaney, J. Savarino, M. M. Frey, and X. Yang (2020), Stratospheric Ozone Changes From Explosive Tropical Volcanoes: Modeling and Ice Core Constraints, *J. Geophys. Res.-Atmos.*, *125*(11), e2019JD032290, doi:https://doi.org/10.1029/2019JD032290.

Morton, J., J. Barnes, B. Schueler, and K. Mauersberger (1990), Laboratory studies of heavy ozone, *J. Geophys. Res.*, *95*(D1), 901-907.

Murray, L. T., L. J. Mickley, J. O. Kaplan, E. D. Sofen, M. Pfeiffer, and B. Alexander (2014), Factors controlling variability in the oxidative capacity of the troposphere since the Last Glacial Maximum, *Atmos. Chem. Phys.*, *14*, 3589-3622.

Nicewonger, M. R., M. Aydin, M. J. Prather, and E. S. Saltzman (2018), Large changes in biomass burning over the last millennium inferred from paleoatmospheric ethane in polar ice cores, *Proc. Natl. Acad. Sci. U. S. A.*, *115*(49), 12413-12418, doi:10.1073/pnas.1807172115.

Nicewonger, M. R., M. Aydin, M. J. Prather, and E. S. Saltzman (2020), Reconstruction of Paleofire Emissions Over the Past Millennium From Measurements of Ice Core Acetylene, *Geophys. Res. Lett.*, *47*(3), e2019GL085101, doi:https://doi.org/10.1029/2019GL085101.

Pfeiffer, M., A. Spessa, and J. O. Kaplan (2013), A model for global biomass burning in preindustrial time: LPJ-LMfire (v1.0), *Geosci. Model Dev.*, *6*(3), 643-685, doi:10.5194/gmd-6-643-2013.

Rind, D., J. Lerner, C. McLinden, and J. Perlwitz (2009), Stratospheric ozone during the Last Glacial Maximum, *Geophys. Res. Lett.*, *36*, L09712.

Rowlinson, M. J., A. Rap, D. S. Hamilton, R. J. Pope, S. Hantson, S. R. Arnold, J. O. Kaplan, A. Arneth, M. P. Chipperfield, P. M. Forster, and L. Nieradzik (2020), Tropospheric ozone radiative forcing uncertainty due to pre-industrial fire and biogenic emissions, *Atmos. Chem. Phys.*, *20*(18), 10937-10951, doi:10.5194/acp-20-10937-2020.

Schoeberl, M. R. (2004), Extratropical stratosphere-troposphere mass exchange, *J. Geophys. Res.*, *109*, D13303, doi:10.1029/2004JD004525.

Škerlak, B., M. Sprenger, and H. Wernli (2014), A global climatology of stratosphere-troposphere exchange using the ERA-Interim data set from 1979-2011, *Atmos. Chem. Phys.*, *14*, 913-937, doi:doi: 10.5194/acp-14-913-2014.

Sofen, E. D., B. Alexander, and S. A. Kunasek (2011), The impact of anthropogenic emissions on atmospheric sulfate production pathways, oxidants, and ice core $\Delta^{17}O$ (SO_4^{2-}), *Atmos. Chem. Phys.*, *11*, 3565-3578, doi:10.5194/acp-11-3565-2011.

Sofen, E. D., B. Alexander, E. J. Steig, M. H. Thiemens, S. A. Kunasek, H. M. Amos, A. J. Schauer, M. G. Hastings, J. Bautista, T. L. Jackson, L. E. Vogel, J. R. McConnell, D. R. Pasteris, and E. S. Saltzman (2014), WAIS Divide ice core suggests sustained changes in the atmospheric formation pathways of sulfate and nitrate since the 19th century in the extratropical Southern Hemisphere, *Atmos. Chem. Phys.*, *14*(11), 5749-5769, doi:10.5194/acp-14-5749-2014.

Thiemens, M. H., and J. E. Heidenreich (1983), The Mass-Independent Fractionation of Oxygen: A Novel Isotope Effect and its Possible Cosmochemical Implications, *Science*, *219*(4588), 1073-1075.

Thiemens, M. H., and T. Jackson (1990), Pressure dependency for heavy isotope enhancement in ozone formation, *Geophys. Res. Lett.*, *17*(6), 717-719, doi:https://doi.org/10.1029/GL017i006p00717.

Thompson, L. G., M. E. Davis, E. Mosley-Thompson, T. A. Sowers, K. A. Henderson, V. S. Zagorodnov, P.-N. Lin, V. N. Mikhalenko, R. K. Campen, J. F. Bolzan, J. Cole-Dai, and B. Francou (1998), A 25,000-Year Tropical Climate History from Bolivian Ice Cores, *Science*, *282*(5395), 1858-1864, doi:10.1126/science.282.5395.1858.

Toon, O. B., H. Maring, J. Dibb, R. Ferrare, D. J. Jacob, E. J. Jensen, Z. J. Luo, G. G. Mace, L. L. Pan, L. Pfister, K. H. Rosenlof, J. Redemann, J. S. Reid, H. B. Singh, A. M. Thompson, R. Yokelson, P. Minnis, G. Chen, K. W. Jucks, and A. Pszenny (2016), Planning, implementation, and scientific goals of the Studies of Emissions and Atmospheric Composition, Clouds and Climate Coupling by Regional Surveys (SEAC^{4}RS) field mission, *J. Geophys. Res.-Atmos.*, *121*(9), 4967-5009, doi:https://doi.org/10.1002/2015JD024297.

Tripati, A. K., S. Sahany, D. Pittman, R. A. Eagle, J. D. Neelin, J. L. Mitchell, and L. Beaufort (2014), Modern and glacial tropical snowlines controlled by sea surface temperature and atmospheric mixing, *Nat. Geosci.*, *7*, 205-209.

Wang, M., Q. Fu, S. Solomon, R. H. White, and B. Alexander (2020), Stratospheric Ozone in the Last Glacial Maximum, *J. Geophys. Res.-Atmos.*, *125*(21), e2020JD032929, doi:https://doi.org/10.1029/2020JD032929.

Wang, Z., J. Chappellaz, K. Park, and J. E. Mak (2010), Large Variations in Southern Hemisphere Biomass Burning During the Last 650 Years, *Science*, *330*(6011), 1663-1666, doi:10.1126/science.1197257.

Wang, Z., E. A. Schauble, and J. M. Eiler (2004), Equilibrium thermodynamics of multiply substituted isotopologues of molecular gases, *Geochim. Cosmochim. Acta*, *68*(23), 4779-4797.

Wiegel, A. A., A. S. Cole, K. J. Hoag, E. L. Atlas, S. M. Schauffler, and K. A. Boering (2013), Unexpected variations in the triple oxygen isotope composition of stratospheric carbon dioxide, *Proc. Natl. Acad. Sci. U. S. A.*, *110*(44), 17680-17685.

Wiegell, M. R., N. W. Larsen, T. Pedersen, and H. Egsdard (1997), The temperature dependence of the exchange reaction between oxygen atoms and dioxygen molecules studied by means of isotopes and spectroscopy, *Int. J. Chem. Kinet.*, *29*(10), 745-753.

Winton, V. H. L., A. Ming, N. Caillon, L. Hauge, A. E. Jones, J. Savarino, X. Yang, and M. M. Frey (2020), Deposition, recycling, and archival of nitrate stable isotopes between the air–snow interface: comparison between Dronning Maud Land and Dome C, Antarctica, *Atmos. Chem. Phys.*, *20*(9), 5861-5885, doi:10.5194/acp-20-5861-2020.

Yeung, L. Y. (2016), Combinatorial effects on clumped isotopes and their significance in biogeochemistry, *Geochim. Cosmochim. Acta*, *172*, 22-38, doi:10.1016/j.gca.2015.09.020.

Yeung, L. Y., H. P. Affek, K. J. Hoag, W. Guo, A. A. Wiegel, E. L. Atlas, S. M. Schauffler, M. Okumura, K. A. Boering, and J. M. Eiler (2009), Large and unexpected enrichment in stratospheric $^{16}O^{13}C^{18}O$ and its meridional variation, *Proc. Natl. Acad. Sci. U. S. A.*, *106*(28), 11496-11501.

Yeung, L. Y., J. L. Ash, and E. D. Young (2014), Rapid photochemical equilibration of isotope bond ordering in O_2, *J. Geophys. Res.*, *119*, 10552-10566, doi:10.1002/2014JD021909.

Yeung, L. Y., J. L. Ash, and E. D. Young (2015), Biological signatures in clumped isotopes of O_2, *Science*, *348*(6233), 431-434, doi:10.1126/science.aaa6284.

Yeung, L. Y., J. A. Hayles, H. Hu, J. L. Ash, and T. Sun (2018), Scale distortion from pressure baselines as a source of inaccuracy in triple-isotope measurements, *Rapid Commun. Mass Spectrom.*, doi:10.1002/rcm.8247.

Yeung, L. Y., L. T. Murray, J. L. Ash, E. D. Young, K. A. Boering, E. L. Atlas, S. M. Schauffler, R. A. Lueb, R. L. Langenfelds, P. B. Krummel, L. P. Steele, and S. D. Eastham (2016), Isotopic ordering in atmospheric O_2 as a tracer of ozone photochemistry and the tropical atmosphere, *J. Geophys. Res.-Atmos.*, *121*, 12,541-512,559, doi:10.1002/2016JD025455.

Yeung, L. Y., L. T. Murray, P. Martinerie, E. Witrant, H. Hu, A. Banerjee, A. Orsi, and J. Chappellaz (2019), Isotopic constraint on the twentieth-century increase in tropospheric ozone, *Nature*, *570*, 224-227, doi:10.1038/s41586-019-1277-1.

Yeung, L. Y., E. D. Young, and E. A. Schauble (2012), Measurements of $^{18}O^{18}O$ and $^{17}O^{18}O$ in the atmosphere and the influence of isotope-exchange reactions, *J. Geophys. Res.*, *117*, D18306, doi:10.1029/2012JD017992.

Young, P. J., A. T. Archibald, K. W. Bowman, J.-F. Lamarque, V. Naik, D. S. Stevenson, S. Tilmes, A. Voulgarakis, O. Wild, D. Bergmann, P. Cameron-Smith, I. Cionni, W. J. Collins, S. B. Dalsøren, R. M. Doherty, V. Eyring, G. Faluvegi, L. W. Horowitz, B. Josse, Y. H. Lee, I. A. MacKenzie, T. Nagashima, D. A. Plummer, M. Righi, S. T. Rumbold, R. B. Skeie, D. T. Shindell, S. A. Strode, K. Sudo, S. Szopa, and G. Zeng (2013), Pre-industrial to end 21st century projections of tropospheric ozone from the Atmospheric Chemistry and Climate Model Intercomparison Project (ACCMIP), *Atmos. Chem. Phys.*, *13*, 2063-2090.